CXCR1 remodels the vascular niche to promote hematopoietic stem and progenitor cell engraftment

Bradley W. Blaser,[1] Jessica L. Moore,[1] Elliott J. Hagedorn,[1] Brian Li,[1] Raquel Riquelme,[1] Asher Lichtig,[1] Song Yang,[1] Yi Zhou,[1] Owen J. Tamplin,[2] Vera Binder,[3] and Leonard I. Zon[1]

[1]Stem Cell Program and Division of Hematology/Oncology, Boston Children's Hospital and Dana Farber Cancer Institute, Howard Hughes Medical Institute, Harvard Medical School, Harvard Stem Cell Institute, Stem Cell and Regenerative Biology Department, Harvard University, Boston, MA 02138
[2]Department of Pharmacology, The University of Illinois College of Medicine, Chicago, IL 60612
[3]Department of Hematology and Oncology, Dr. von Hauner Children's Hospital, Ludwig-Maximilians University, 80539 Munich, Germany

The microenvironment is an important regulator of hematopoietic stem and progenitor cell (HSPC) biology. Recent advances marking fluorescent HSPCs have allowed exquisite visualization of HSPCs in the caudal hematopoietic tissue (CHT) of the developing zebrafish. Here, we show that the chemokine *cxcl8* and its receptor, *cxcr1*, are expressed by zebrafish endothelial cells, and we identify *cxcl8/cxcr1* signaling as a positive regulator of HSPC colonization. Single-cell tracking experiments demonstrated that this is a result of increases in HSPC–endothelial cell "cuddling," HSPC residency time within the CHT, and HSPC mitotic rate. Enhanced *cxcl8/cxcr1* signaling was associated with an increase in the volume of the CHT and induction of *cxcl12a* expression. Finally, using parabiotic zebrafish, we show that *cxcr1* acts HSPC nonautonomously to improve the efficiency of donor HSPC engraftment. This work identifies a mechanism by which the hematopoietic niche remodels to promote HSPC engraftment and suggests that *cxcl8/cxcr1* signaling is a potential therapeutic target in patients undergoing hematopoietic stem cell transplantation.

INTRODUCTION

The hematopoietic microenvironment is a critical regulator of hematopoietic stem and progenitor cell (HSPC) function under normal conditions, in the presence of malignancy, and under conditions of stress such as regeneration after cytotoxic chemotherapy and engraftment after hematopoietic stem cell transplantation (HSCT; Krause and Scadden, 2012; Morrison and Scadden, 2014). Within the hematopoietic microenvironment there are several niches, each of which hosts cell types with distinct functional roles in the biology of one or more subsets of HSPCs. The vascular niche and the osteoblastic niche have long been appreciated to be important for supporting hematopoietic stem cell (HSC) biology. Elegant work using tissue-specific knockout mice has shown that the vascular niche is indispensable for HSC maintenance and regeneration, whereas the osteoblastic niche is critical for supporting a subset of lymphoid progenitors (Zhu et al., 2007; Hooper et al., 2009; Ding et al., 2012; Ding and Morrison, 2013; Morrison and Scadden, 2014). Within the vascular niche, the arteriolar niche is thought to contain quiescent $NG2^{+}Nestin^{bright}\alpha$-smooth muscle $actin^{+}$ perivascular stromal cells that express high levels of CXCL12/SDF-1 and maintain HSCs in a state of quiescence under steady-state conditions (Kunisaki et al., 2013). In contrast, the sinusoidal niche is composed of $VEGFR2^{+}VEGFR3^{+}$ sinusoidal endothelial cells and $Nestin^{dim}Lepr^{+}$ perivascular stromal cells that express a large number of secreted molecules including Notch ligands, CXCL12/SDF-1, BMP ligands, stem cell factor (SCF), and others (Fernandez et al., 2008; Butler et al., 2010; Ding et al., 2012; Ding and Morrison, 2013). The sinusoidal niche is a dynamic locale with angiogenesis and hematopoietic regeneration occurring in concert after myelotoxic stress. Without an intact sinusoidal vascular niche in the marrow, long term hematopoietic repopulation after myeloablation and HSCT is severely compromised (Hooper et al., 2009). Likewise, the sinusoidal niche is necessary for hematopoiesis in the spleen under conditions of stress such as recovery from chemotherapy, pregnancy, and blood loss (Inra et al., 2015). A complete understanding of the mechanisms by which the sinusoidal niche regulates hematopoiesis during stress will bring to light new therapies that can improve hematopoietic reconstitution.

Recently, we identified an enhancer element for the transcription factor *Runx1* that specifically marks HSCs in the developing zebrafish that have long-term hematopoietic repopulating capacity (Tamplin et al., 2015). Using *Runx1* transgenic reporter lines, we identified a novel interaction between HSCs and sinusoidal endothelial cells during a period of development characterized by dynamic changes in

Correspondence to Leonard I. Zon: zon@enders.tch.harvard.edu

Abbreviations used: AGM, aorta-gonad-mesonephros; CHT, caudal hematopoietic tissue; dpf, d post fertilization; EET, epoxyeicosatrienoic acid; GSEA, gene set enrichment analysis; hpf, h post fertilization; HSC, hematopoietic stem cell; HSCT, hematopoietic stem cell transplantation; HSPC, hematopoietic stem and progenitor cell; PGE2, prostaglandin E2; VEGF, vascular endothelial growth factor; WISH, whole mount in situ hybridization.

The Rockefeller University Press $30.00
J. Exp. Med. 2017 Vol. 214 No. 4 1011–1027
https://doi.org/10.1084/jem.20161616

the niche and expansion of the HSC pool (Tamplin et al., 2015). *Runx1*$^+$ HSCs arise from endothelial cells in the aorta-gonad-mesonephros (AGM) region and enter circulation; beginning around 36 h after fertilization (hpf), they colonize the caudal hematopoietic tissue (CHT), a vascular plexus in the tail of the zebrafish embryo (Murayama et al., 2006). HSCs adhere to the luminal surface of the sinusoidal endothelial cells, transmigrate to the extraluminal space and there they interact intimately with components of the niche including endothelial cells, stromal cells, and possibly other cells, in a process known as "cuddling" (Tamplin et al., 2015; Mahony et al., 2016). HSCs undergo rapid expansion within this temporary niche until ∼6 d post fertilization (dpf), when they migrate to the kidney marrow where they remain for the life of the animal (Chen and Zon, 2009).

Here, we sought to identify the molecular factors that mediate HSPC interactions with the sinusoidal endothelial cells of the CHT niche. Using gene expression studies, gain- and loss-of-function genetics and single-cell track analysis, we show that *cxcl8/cxcr1* signaling increases endothelial cell cuddling and enhances expression of *cxcl12a/sdf-1a* leading to increased HSPC residency time within the niche. These effects allow for additional HSPC cell divisions to occur with a consequent increase in CHT colonization. Using digital reconstruction of the CHT and a parabiotic zebrafish system, we show that *cxcl8/cxcr1* signaling positively regulates both CHT volume and HSPC engraftment in a stem cell nonautonomous manner. Collectively, these data identify a new role for *cxcl8/cxcr1* in remodeling the sinusoidal vascular niche during the process of HSPC colonization in the developing zebrafish. Further, they suggest that modulation of CXCL8/CXCR1 signaling may be beneficial in recipients of HSCT.

RESULTS

Cxcl8 and cxcr1 are expressed by zebrafish endothelial cells and enhance HSPC colonization

To identify genes that might be involved in HSPC–endothelial cell interactions, endothelial cells and HSPCs were sorted from *Tg(kdrl:mCherry;Runx1+23:GFP)* transgenic zebrafish embryos at 72 h after fertilization (hpf) and from the kidney marrow of adult transgenic zebrafish. The *kdrl (vegfr2)* and murine *Runx1* enhancer/promoter elements specifically mark zebrafish endothelial cells and HSPCs, respectively (Jin et al., 2005; Chi et al., 2008; Tamplin et al., 2015). We undertook gene expression profiling on all four populations (adult and embryonic mCherry$^+$ endothelial cells and GFP$^+$ HSPCs) by microarray analysis (Affymetrix Zebrafish 1.0 ST array). To identify sets of genes with differential expression between endothelial cells and HSPCs, we searched the NCBI Gene database for keywords representing 18 categories of extracellular and secreted molecules in the zebrafish genome (Fig. S1). The number of unique genes across all gene sets was 1,900. Some genes were present in more than one gene set; accounting for this overlap, 2462 gene set entries were created. Table S1 lists all 2462 gene set entries ordered by gene set with Entrez unique identifier and gene symbol, if annotated. Gene set enrichment analysis (GSEA; Subramanian et al., 2005) was then performed using these gene sets and the adult and embryonic gene expression data to identify gene sets enriched in the endothelial cell phenotype relative to the HSPC phenotype. In this analysis, the zebrafish chemokine gene set had the most significant enrichment in both adult and embryonic endothelial cells ($P = 0.000$ for both comparisons, Fig. 1 a and Tables S2 and S3). The intersection of the leading-edge chemokine genes in the embryonic and adult datasets contained 20 genes (Fig. 1 b and Tables S4–S6). 16 of these 20 chemokine genes were subsequently used as candidates in a gain-of-function screen.

Candidate chemokine genes were expressed at high levels in F_0 mosaic transgenic zebrafish by microinjecting single-cell embryos with DNA encoding the candidate gene under the control of the heat shock–inducible promoter for *hsp70l* (Adám et al., 2000; Halloran et al., 2000). Heat shock induction was performed at 36 and 48 hpf, coincident with the initial wave of HSPC colonization of the CHT. This approach resulted in >20-fold overexpression of the candidate genes compared with animals that did not undergo heat shock induction (Fig. S2). Whole-mount in situ hybridization (WISH) was performed using a mixture of probes marking HSPCs (*runx1/c-myb*), followed by blinded scoring for HSPC colonization of the CHT. Embryos injected with DNA encoding GFP under the same *hsp70l* promoter served as a control (Fig. 1 c). Mosaic overexpression of *cxcr1* (loc797181) enhanced HSPC colonization in this assay ($P = 0.033$; $n = 63$ embryos; Fig. 1, d and e). The ligand for *cxcr1* in humans, *cxcl8*, similarly enhanced HSPC colonization of the CHT ($P = 0.0028$; $n = 41$ embryos; Fig. 1, f and g).

WISH for zebrafish *cxcr1* in wild-type embryos revealed a diffuse low-level staining pattern with specific enhancement in the CHT (Fig. 1, h and i). Expression of both *cxcr1* and *cxcl8* was detected by RT-PCR in *kdrl:mCherry*$^+$ endothelial cells sorted from embryos at 72 hpf (Fig. 1 j). Neither *cxcr1* nor *cxcl8* were detectable in sorted HSPCs at the mRNA level (unpublished data). Sorted endothelial cells were treated for 30 min in vitro with 11,12-epoxyeicosatrienoic acid (EET), a small arachidonic acid derivative recently shown by our laboratory to enhance HSC engraftment in embryonic zebrafish and in adult zebrafish and murine HSCT assays (Li et al., 2015; Tamplin et al., 2015). This brief treatment enhanced endothelial cell *cxcl8* expression by approximately sixfold and *cxcr1* expression by approximately threefold (Fig. 1, k and l). Thus, *cxcr1* and *cxcl8* are present within the endothelial cell niche early during its development and both are inducible by a compound known to play a role in promoting hematopoiesis.

To quantitate the effects of *cxcr1* and *cxcl8* on HSPC colonization, we performed gain- and loss-of-function experiments in the *Tg(Runx1+23:NLS-mCherry)* HSPC transgenic reporter line (referred to hereafter as *Runx1:mCherry*; Tamplin et al., 2015). Mosaic, high-level gene

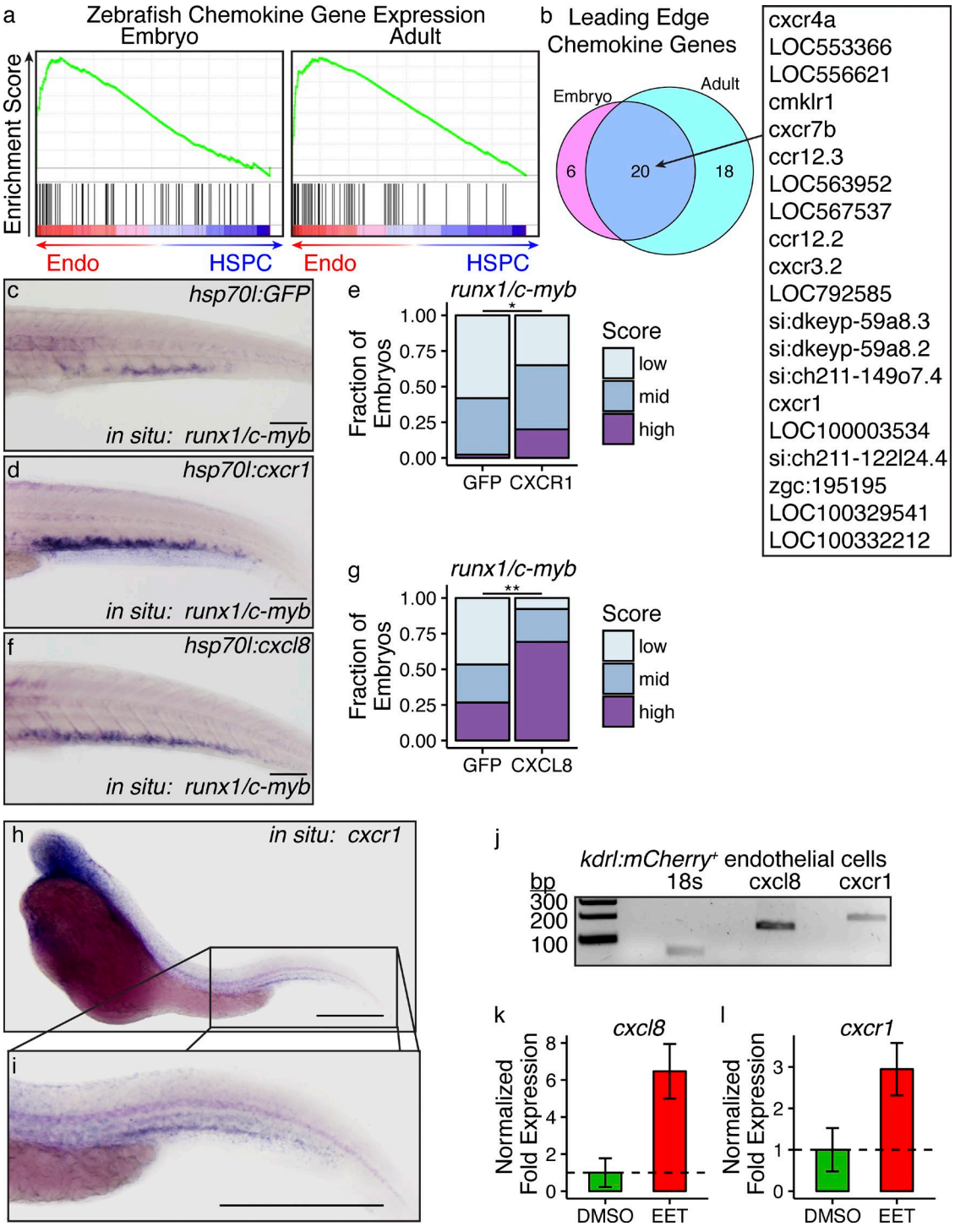

Figure 1. **Gene expression profiling and a gain-of-function screen identify potential regulators of HSPC colonization.** (a) GSEA enrichment plots for the chemokine gene set in embryonic and adult endothelial cells and HSCs. In both plots, genes enriched in endothelial cells are plotted to the left and genes enriched in HSCs are plotted to the right (P = 0.000 for both comparisons). (b) Overlap of the leading-edge chemokine genes from the embryonic and adult GSEA. (c–g) Leading edge genes were induced by heat shock at 36 and 48 hpf, followed by fixation at 72 hpf and WISH using a mix of *runx1/c-myb* probes to mark HSCs and HSPCs. Representative animals injected with heat shock inducible plasmids encoding GFP (c), *cxcr1* (d), and *cxcl8* (f) are shown. Bars, 100 µm. Bar plots (e and g) show blinded scoring data for *runx1/c-myb* staining in the CHT of CXCR1 (e) and CXCL8 (g) groups compared with GFP control (Wilcoxon rank sum test, P = 0.033, *n* = 43 for GFP control, and *n* = 20 for CXCR1; P = 0.0028; *n* = 15 for GFP control and *n* = 26 for CXCL8). Both experiments were repeated twice with similar results. Representative experiments are shown. To account for clutch-to-clutch variability in staining, all experimental groups were compared only to controls from the same clutch. (h and i) WISH for *cxcr1* expression in a WT 48 hpf embryo. The images are

expression was induced in F_0 transgenic animals injected with DNA encoding *hsp70l:cxcr1* or *hsp70l:GFP* by heat shock at 36 and 48 hpf. Stable transgenic lines (F_1 generation) did not tolerate heat shock induction of *cxcr1*, likely because the transgene was expressed at toxic levels. The entire CHT was imaged at 72 hpf by fluorescence confocal microscopy (Fig. 2 a, black box). Digital image analysis (Imaris; Bitplane Scientific) was used for unbiased image segmentation and classification of spots by a composite measure of fluorescence intensity, size and roundness. The threshold for identifying HSPCs from background fluorescence was set such that ∼3–8 such spots were present in the control group, a number known to be present in this transgenic line based on limiting dilution experiments and imaging of the entire CHT (Tamplin et al., 2015). The same thresholds were then used to segment and classify spots as HSPCs in experimental groups. Fig. 2 (b_i and c_i) shows the raw fluorescence images from a portion of the CHT (denoted by the red box in Fig. 2 a). Fig. 2 (b_{ii} and c_{ii}) shows the HSPCs as identified by unbiased digital analysis, and Fig. 2 (b_{iii} and c_{iii}) shows an overlay of the fluorescence images and segmented spots. Mosaic overexpression of *cxcr1* beginning at 36 hpf increased HSPC colonization of the CHT at 72 hpf (3.8 ± 1.0 vs. 9.1 ± 1.9 HSPCs per CHT; P = 0.020, Fig. 2 d). HSC specification in the AGM requires *cxcl8* expression and so this experiment was repeated with heat shock induction at 48 and 60 hpf, a period of time after peak HSC specification but still during the initial wave of CHT colonization (Jing et al., 2015). HSPC colonization of the CHT was enhanced by *cxcr1* under these conditions as well (4.3 ± 0.9 vs. 11.8 ± 3.1 HSPCs per CHT, P = 0.023, Fig. 2, e–g).

Next, to understand the requirement for *cxcl8* in HSPC colonization of the CHT, we bred the *Runx1:mCherry* reporter transgene into animals carrying a loss-of-function missense mutation in *cxcl8* (*cxcl8*$^{-/-}$ (Jing et al., 2015)). *Runx1:mCherry;cxcl8*$^{+/-}$ animals were incrossed and the progeny imaged at 72 hpf, followed by genotyping for *cxcl8*. *Runx1:mCherry;cxcl8*$^{+/+}$ animals had significantly higher HSPC colonization of the CHT compared with *Runx1:mCherry;cxcl8*$^{-/-}$ clutchmates (7.2 ± 1.4 vs. 2.6 ± 0.7 HSPCs per CHT, P = 0.02, Fig. 2, h–k). There was no significant difference between *Runx1:mCherry;cxcl8*$^{+/-}$ animals and either wild-type or mutant clutchmates.

Finally, we wished to understand if a related chemokine receptor, *cxcr2* (loc796724), would similarly enhance HSPC colonization. Global overexpression of zebrafish *cxcr2* beginning at 36 hpf did not increase HSPC colonization when tested in this assay (Fig. 2 l).

CXCL8 and other immune mediators such as IL-6, IFN-γ, TNF, prostaglandin E_2 (PGE_2), and EET may have a role in directly stimulating HSC emergence from the AGM (North et al., 2007; Kobayashi et al., 2010; Espín-Palazón et al., 2014; Sawamiphak et al., 2014; Jing et al., 2015; Li et al., 2015). *Cxcl8* morphants and *cxcl8*$^{-/-}$ mutants have reduced numbers of HSCs in the AGM (Jing et al., 2015). Although induction of *cxcr1* in our gain-of-function experiments begins at the end of AGM hematopoiesis, it is possible that enhanced HSC specification and emergence might contribute to the increased numbers of HSPCs seen in the CHT. To rule out this possibility, *Tg(sclβ:GFP;kdrl:mCherry)* animals were generated and *cxcr1* expression was induced at 36 hpf by DNA microinjection and heat shock. The AGM was imaged from 38–49 hpf by time-lapse video microscopy and emerging *sclβ:GFP*$^{+}$ HSPCs were identified as they budded from the floor of the dorsal aorta into the AGM (Kissa and Herbomel, 2010; Zhen et al., 2013; Jing et al., 2015; Fig. 3, a–e). The number of HSPCs per somite over this period is plotted in Fig. 3 f. Induction of *cxcr1* caused no significant increase in HSC emergence compared with animals injected with control DNA encoding an empty vector or uninjected animals treated with DMSO. In contrast, animals treated with PGE_2 as a positive control beginning at 16-somite stage had significantly higher numbers of HSPCs per somite compared with the other groups. Collectively, these experiments using gain- and loss-of-function genetic techniques demonstrate a new and independent role for *cxcl8/cxcr1* signaling in supporting HSPC colonization of the CHT.

cxcr1 enhances CHT residency time and endothelial cell cuddling of HSPCs

We next aimed to understand the cellular mechanisms by which *cxcr1* supports HSPC colonization. Heat shock induction of *cxcr1* gene expression was performed at 36 and 48 hpf, followed by time-lapse fluorescence microscopy of *Runx1:mCherry* embryos from 52 to 72 hpf. Digital image analysis was performed, as previously described, and HSPCs were enumerated over these 20 h. Mosaic overexpression of *cxcr1* had little effect on HSPC numbers within the CHT until ∼55 hpf, after which there were consistently more HSPCs in animals expressing *cxcr1* compared with GFP control (Fig. 4 a). As our previous experiments had suggested that AGM hematopoiesis was not enhanced by *cxcr1* under these conditions, we hypothesized that the increased numbers of HSPCs in the CHT of these animals would be due in part to increased retention time within the niche itself. Single-cell track analysis was performed to determine the residency time of individual HSPCs within the CHT (n = 648 tracks analyzed, Fig. 4 b). Control animals expressing GFP showed a distribution of residency times with the large majority of cell tracks lasting <6 h, consistent with previously published

representative of two separate clutches. Bars, 700 µm. (j) Expression of *cxcl8* and *cxcr1* mRNA in endothelial cells freshly sorted from 72 hpf *kdrl:mCherry* embryos. (k and l) Sorted endothelial cells were treated with EET or DMSO (control) for 30 min before assessment of *cxcl8* (k) and *cxcr1* (l) expression by qRT-PCR. Experiments in j–l were repeated twice, with similar results.

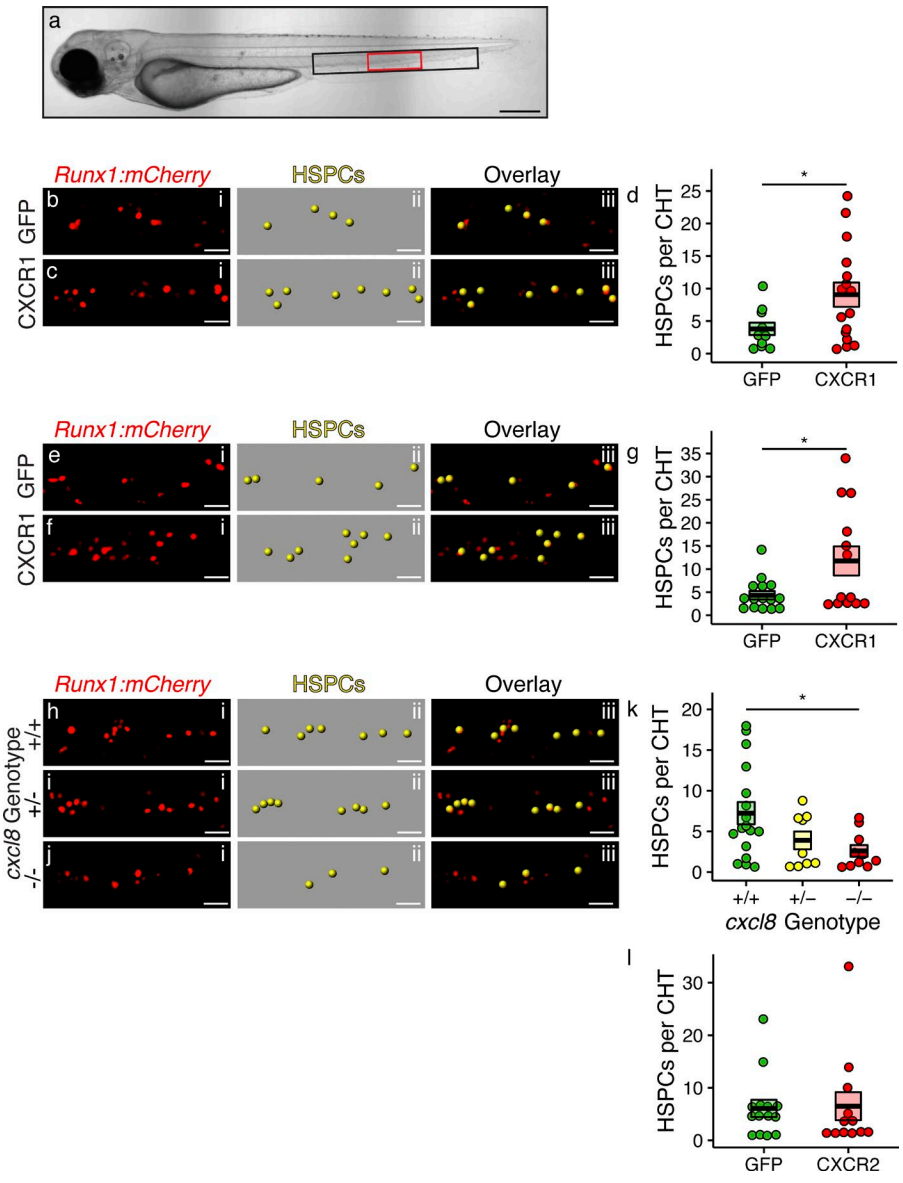

Figure 2. **Cxcl8/cxcr1 signaling is a positive regulator of HSPC colonization.** (a) Transmitted light image of a 72 hpf embryo. HSCs and HSPCs were enumerated in the entire CHT (black box) using digital image analysis as described in the text. The red box shows the approximate area selected for the representative images below. Bar, 300 µm. (b–d) GFP or *cxcr1* was overexpressed by heat shock induction at 36 and 48 hpf and HSPC colonization of the CHT was quantified at 72 hpf. Representative fluorescence images (b_i and c_i), digital image segmentation (b_{ii} and c_{ii}), and overlays (b_{iii} and c_{iii}) are shown. (d) GFP and CXCR1 groups were compared using Student's *t* test (P = 0.020, *n* = 10 for GFP control; *n* = 16 for CXCR1). The experiment was repeated twice; combined results are shown. (e–g) GFP or *cxcr1* was overexpressed as in panels b-d except that heat shock induction was performed at 48 and 60 hpf with imaging at 84 hpf (P = 0.023, Student's *t* test, *n* = 15 for GFP control and *n* = 13 for CXCR1). The experiment was repeated twice; combined results are shown. (h–k) Runx*1:mCherry;cxcl8*$^{+/-}$ animals were in-crossed to generate *Runx1:mCherry;cxcl8*$^{+/+}$ (h), *Runx1:mCherry;cxcl8*$^{+/-}$ (i), and *Runx1 :mCherry;cxcl8*$^{-/-}$ (j) animals. Animals were imaged at 72 hpf and HSPC colonization of the CHT was quantified (k; P = 0.02 for the comparison of +/+ and –/– groups; Student's *t* test; *n* = 17 for +/+, *n* = 9 for +/–, and *n* = 10 for –/– groups). The experiment was repeated four times; combined results are shown. Bars, 20 µm. (l) Expression of GFP or *cxcr2* was induced by heat shock at 36 and 48 hpf, as before. Animals were imaged at 72 hpf, and HSPCs were enumerated in the CHT. Groups were compared using Student's *t* test (p = NS; *n* = 14 for GFP control and *n* = 12 for *cxcr2*). The experiment was repeated twice with similar results; combined results are shown.

results (Tamplin et al., 2015). In contrast, animals expressing *cxcr1* had an expanded number of cell tracks lasting between 7 and 15 h, increasing the residency time of the top 10% of HSPCs by nearly 2 h (Fig. 4 b, dashed lines). These long-term resident HSPCs in animals overexpressing *cxcr1* significantly increased the mean residency time of this group compared with control (3.0 ± 0.1 vs. 3.4 ± 0.2 h, P = 0.029).

After the observation of increased CHT residency time in animals overexpressing *cxcr1*, it next seemed likely that HSPCs in these animals would have the opportunity to undergo additional rounds of cell division while within the niche. Mitotic events were enumerated in the time lapse datasets, and it was found that HSPCs in animals overexpressing *cxcr1* were 1.8-fold more likely to undergo mitosis relative to GFP control (0.31 ± 0.05 vs. 0.56 ± 0.08 mitoses per HSPC, P = 0.0041, Fig. 4, c and d). The increased number of HSPC cell divisions was not only a consequence of residency time, as overexpression of *cxcr1* also increased the intrinsic rate of HSPC mitosis by 1.5-fold (0.07 ± 0.01 vs. 0.11 ± 0.02 mitoses/HSPC/hour within the CHT, P = 0.02, Fig. 4 e). Finally, we hypothesized that endothelial cell cuddling would be increased in association with the effects on CHT retention time and HSPC mitosis seen in these time-lapse experiments. To test this hypothesis, *cxcr1* was overexpressed in *Runx1 :mCherry;kdrl:GFP* double transgenic animals, and cuddling events were identified as shown in the still frames in Fig. 4 f (*n* = 468 total tracks evaluated; Video 1). In this example, the HSPC identified by the arrow is in transit from 51–52 hpf and remains cuddled in an endothelial cell pocket from 52–59 hpf before exiting. Fig. 4 f_{vi} shows mitosis of this cell and

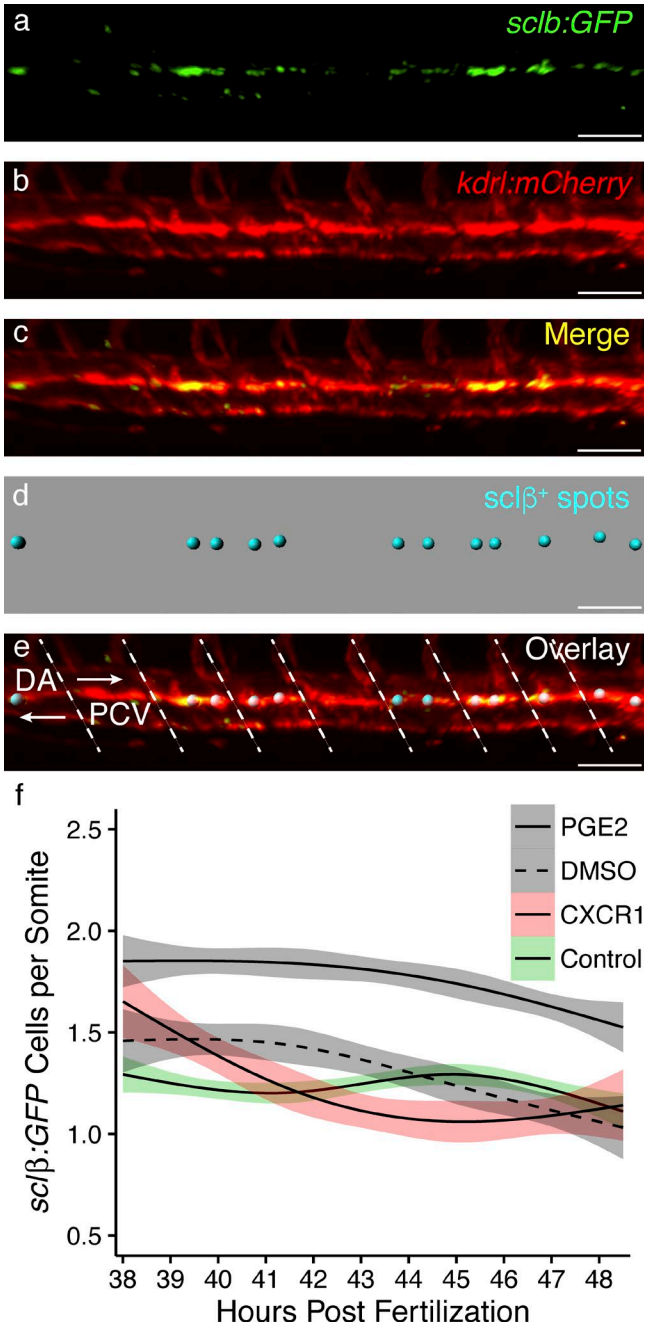

Figure 3. **Induction of cxcr1 at 36 hpf does not enhance HSPC emergence.** *Scl-β:GFP;kdrl:mCherry* transgenic animals were injected with DNA encoding *cxcr1* or empty vector (Control) and gene expression was induced by heat shock at 36 hpf. Uninjected animals were treated with DMSO or PGE_2 beginning at the 16-somite stage and served as additional negative and positive controls. The AGM region was imaged from 38–49 hpf. (a–e) Representative fluorescence images showing *scl*β*-GFP* (a), *kdrl :mCherry* (b), merged GFP and mCherry channels (c), *scl*β$^+$ spots identified by digital image analysis and an overlay image with somite boundaries and dorsal aorta (DA) and posterior cardinal vein (PCV) marked (e). Bar = 70 µm. (f) Time series plot showing the cumulative numbers of *scl*β*:GFP*$^+$ cells in the AGM of each group (n = 9 for PGE2, n = 5 for DMSO, n = 10 for control, and n = 6 for CXCR1). Colored bands represent 95% confidence intervals. The experiment was repeated twice with similar results; a representative experiment is shown.

release of a daughter cell (arrowhead) from the pocket. The percent cuddling time relative to overall time each HSPC spent in the CHT was significantly increased in animals overexpressing *cxcr1* compared with control animals (40.1 ± 2.3 vs. 66.2 ± 4.5% cuddling time; $P = 6.28 \times 10^{-7}$; Fig. 4 g). Collectively, these findings show that *cxcl8/cxcr1* signaling acts as an overall positive regulator of CHT colonization in the developing zebrafish. This effect is likely a consequence of enhanced interactions with the sinusoidal endothelial cell niche, leading to prolonged retention time, increased rate of HSPC mitosis, and an overall expansion of the HSPC pool.

Cxcr1 induces functional and structural changes in the endothelial cell niche that favor HSPC colonization

To better understand the mechanisms by which *cxcr1* acts on the endothelial cell niche to enhance HSPC colonization, we generated a stable transgenic line expressing *cxcr1* under the control of the endothelial cell-specific promoter, *kdrl (Tg(kdrl:cxcr1),* hereafter referred to as *kdrl:cxcr1).* Expression of *cxcr1* in sorted endothelial cells from these transgenic embryos was roughly 2.4-fold higher than in endothelial cells from WT clutchmates by quantitative PCR (Fig. 5 a). There were no significant differences in expression of other angiogenesis-related genes in sorted endothelial cells by RNA sequencing. *Runx1:mCherry;kdrl:cxcr1* double transgenic animals were imaged at 72 hpf and found to have significantly increased HSPC colonization of the CHT compared with *Runx1:mCherry* clutchmates without the *cxcr1* transgene (6.1 ± 1.1 vs. 10.8 ± 1.2 HSPCs per CHT; P = 0.001, Fig. 5, b–d). *Mpx:GFP;kdrl:cxcr1* transgenic animals did not have increased numbers of mature neutrophils within the CHT suggesting that overexpression of *cxcr1* does not enhance colonization of all myeloid cell types (Fig. 5 e).

CXCL12 (SDF-1) is a chemokine ligand expressed by endothelial and perivascular stromal cells that is essential for HSC maintenance and engraftment after transplantation (Nagasawa et al., 1996; Ara et al., 2003; Sugiyama et al., 2006; Ding and Morrison, 2013; Inra et al., 2015). Enforced expression of CXCL12 by endothelial cells in $CXCL12^{-/-}$ mice is sufficient to rescue a profound defect in HSC numbers in the bone marrow (Ara et al., 2003). We therefore hypothesized that the increased numbers of HSPCs in *kdrl :cxcr1* transgenics might be associated with induction of *cxcl12* in the CHT. Zebrafish *cxcl12* exists in two isoforms, *cxcl12a* and *cxcl12b*, both of which have critical roles in embryonic hematopoiesis (Zhang et al., 2011; Nguyen et al., 2014; Tamplin et al., 2015). Overexpression of *cxcr1* in *kdrl:cxcr1* transgenic animals increased expression of *cxcl12a* within the CHT compared with WT clutchmates by WISH (P = 0.03; n = 60 embryos, Fig. 5, f–h) whereas expression of *cxcl12b*

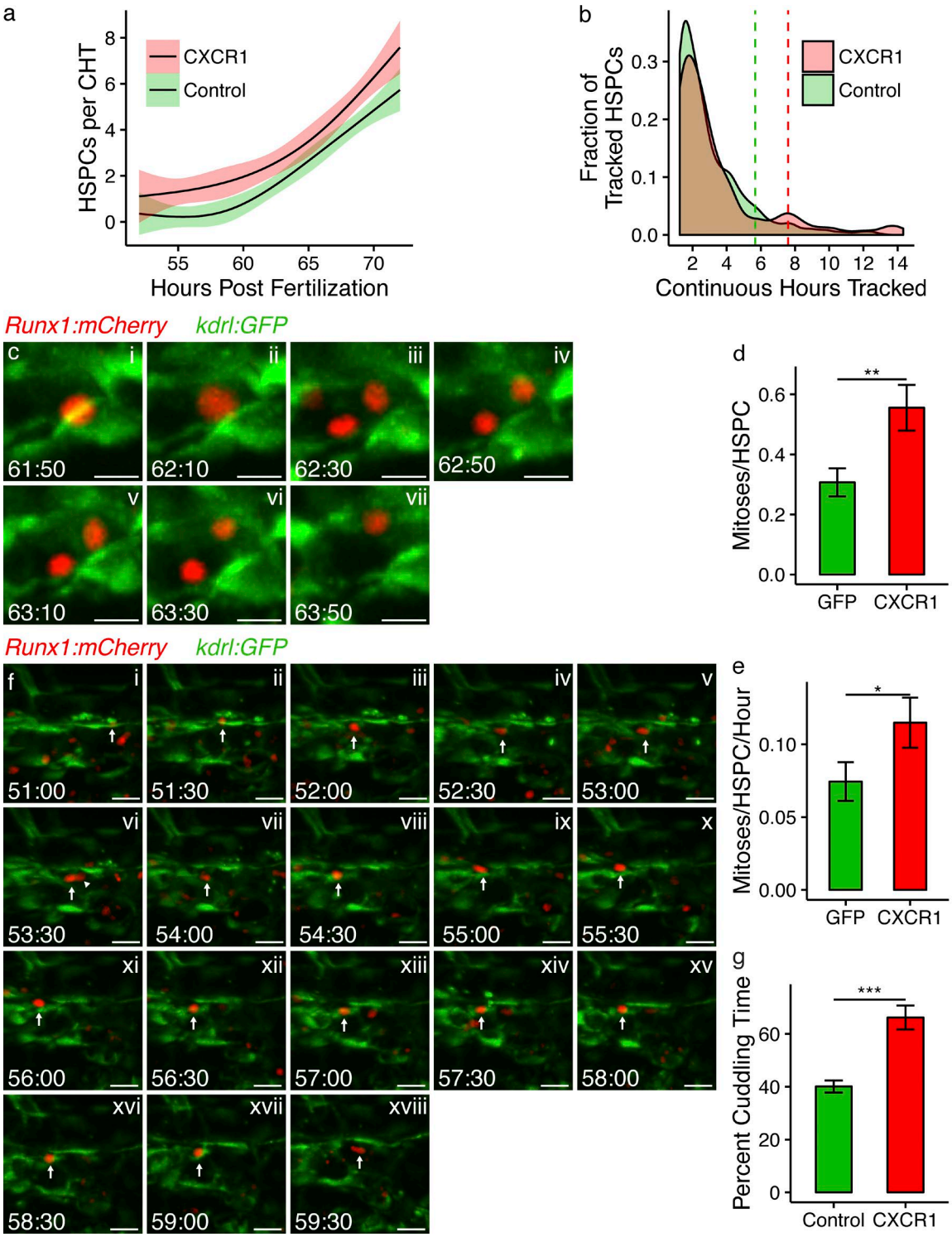

Figure 4. **Overexpression of cxcr1 increases HSPC residency time, mitotic rate and endothelial cell cuddling within the CHT.** (a–e) *Runx1:mCherry* or *Runx1:mCherry;kdrl:GFP* zebrafish embryos were microinjected with DNA encoding *hsp70l:cxcr1* or control DNA *(hsp70l:GFP* or empty vector*)*, gene expression was induced by heat shock at 36 and 48 hpf, and HSPC colonization of the CHT was quantified by time lapse video microscopy from 52 to 72 hpf. (a) Time series plot showing the number of HSPCs in each group (n = 7 for Control and n = 5 for CXCR1). Colored bands represent 95% confidence intervals. The experiment was repeated twice with similar results; a representative experiment is shown. (b) Cumulative density function showing the fraction of HSPCs tracked in the CHT for any duration of time. The area under the curve between any two points on the x-axis represents the fraction of HSPCs continuously tracked for that length of time. Dashed lines represent the lower limit of the 10% of cells with the longest CHT residency time (CXCR1

was unaffected (Fig. 5, i–k). This suggests that *cxcr1* modifies the function of the niche to favor HSPC colonization.

To look specifically at the response of endothelial cells to *cxcr1* stimulation, primary human umbilical vein endothelial cells (HUVECs) were treated for 6 h in vitro with purified recombinant human CXCL8 (rhCXCL8, RND systems). This brief treatment induced endothelial cell CXCL12 mRNA expression by 1.5-fold compared with control (Fig. 5 l). Expression of survivin and VEGFA, known targets of CXCL8/CXCR1 in endothelial cells, was induced by 2.4- and 1.5-fold, respectively (Fig. 5 l; Li et al., 2003). In addition, rhCXCL8 treatment induced expression of CXCL8 itself (Fig. 5 l). After 24 h in culture, VEGF protein was undetectable in the culture supernatants of control-treated cells but could be detected at low levels in cells treated with rhCXCL8 (4.8 ± 0.86 pg/ml). There was no difference in CXCL12 levels in culture supernatants (22.8 ± 1.1 vs. 24.4 ± 0.97 pg/ml). RNA sequencing and IPA analysis were performed to understand the global gene expression changes induced by CXCL8/CXCR1 signaling (Fig. 5 m). The induction of anti-apoptotic and angiogenic factors (survivin and VEGFA) as well as the global gene expression changes in favor of cellular maintenance and movement suggested the possibility that CXCL8/CXCR1 signaling might cause structural reorganization or expansion of the niche that could provide space for additional HSPC colonization.

To address this hypothesis, *cxcr1* expression was induced at 36 and 48 hpf in wild-type zebrafish embryos using the heat shock-inducible system and the structure of endothelial cell niche was assessed by WISH for the endothelial cell marker, *kdrl*. Overexpression of *cxcr1* increased the size and intensity of *kdrl* staining in a blinded scoring assay ($P = 0.041$; $n = 40$; Fig. 6, a–c). The larger vasculature was grossly unaffected. To measure the effect of *cxcr1* on the size of the niche directly, *cxcr1* expression was induced by DNA microinjection and heat shock induction in *Tg(kdrl:GFP)* or *Tg(kdrl:hRAS-mCherry;* hereafter referred to as *kdrl:GFP* and *kdrl:mCherry*) reporter zebrafish as before. Animals were imaged by confocal microscopy at 72 hpf (Fig. 6 d). The CHT was then digitally reconstructed in three dimensions and its volume measured using Imaris digital image analysis software (Fig. 6, e and f). Induction of *cxcr1* expression increased the volume of the CHT by 26% compared with animals that did not undergo heat shock induction (1.06 ± 0.08 vs. 1.34 ± 0.07 × 10^6 μm^3; $P = 0.02$, Fig. 6 g). Treatment of *kdrl:mCherry* transgenics with the selective inhibitor of CXCR1/CXCR2, SB225002 (Cayman Chemical), from 48 to 72 hpf reduced CHT volume at 72 hpf (8.91 ± 0.49 vs. 6.4 ± 0.70 × 10^5 μm^3; $P = 0.012$; Fig. 6 h). These findings at static time points were confirmed by measuring CHT volume continuously from 52 to 72 hpf using time-lapse video microscopy. Overexpression of *cxcr1* beginning at 36 hpf progressively increased CHT volume from 53 hpf onward (Fig. 6 i). To look specifically at the effect of *cxcr1* expression in the endothelial cell compartment on the volume of the niche, we again used the *kdrl:cxcr1* transgenic line. Double transgenic *kdrl:cxcr1;kdrl:mCherry* animals were generated and were found to have significantly greater CHT volume compared with *kdrl:mCherry* clutchmates (1.1 ± 0.05 vs. 1.3 ± 0.06 × 10^6 μm^3; $P = 0.02$; Fig. 6 j). Finally, we wished to confirm these findings in an independent reporter line. Lymphatic vessel endothelial hyaluronan receptor 1b (*lyve1b*) is expressed in lymphatic vessels and in the CHT at 72 hpf (Fig. 6, k–p; Flores et al., 2010; Okuda et al., 2012). The *Tg(lyve1b:GFP;* referred to as *lyve1b:GFP*) line was crossed to the *kdrl:cxcr1* line to generate *lyve1b:GFP;kdrl:cxcr1* and *lyve1b:GFP* (referred to as WT) clutchmates, followed by imaging of the CHT at 72 hpf. Embryos carrying the *kdrl:cxcr1* transgene had a significantly larger CHT compared WT control embryos (5.3 ± 0.17 vs. 6.3 ± 0.18 × 10^5 μm^3; $P = 0.0006$; Fig. 6 p). These findings demonstrate that in concert with induction of *cxcl12a* expression, *cxcr1* induces structural changes that support HSPC colonization within the sinusoidal vascular niche.

Cxcr1 acts stem cell nonautonomously to enhance HSPC engraftment in parabiotic zebrafish

We aimed to better understand the cell autonomy of the effects of *cxcr1* on HSPC engraftment. To do this, pairs of zebrafish embryos were fused at 4 hpf to create parabiotic organisms (Demy et al., 2013; Murayama et al., 2015; Hagedorn et al., 2016). All parabiotics used in these experiments developed

in red, Control in green). $n = 10$ animals, 461 total tracked HSPCs for Control and $n = 6$ animals, 187 total tracked HSPCs for CXCR1, $P = 0.029$ (Student's *t* test). The experiment was repeated twice with similar results; combined results are shown. (c–e) Tracked HSPCs were followed and mitotic events were enumerated. (c) A representative mitotic event in a *Runx1:mCherry;kdrl:GFP* transgenic injected with DNA encoding *hsp70l:cxcr1*. HSPCs undergoing mitosis were observed to reduce their migration (c_i) and undergo nuclear cleavage (c_{ii}–c_{iii}), often rotating in the process, followed by release of the daughter cell (c_{vii}). Bars, 10 μm. The number of mitotic events per HSPC is plotted in (d; $P = 0.0041$, Student's *t* test) and the number of mitotic events per HSPC per hour of CHT residency time for that HSPC is plotted in (e; $P = 0.02$, Wilcoxon's rank sum test). $n = 6$ animals, 122 total tracked HSPCs for GFP/Control and $n = 5$ animals, 107 total tracked HSPCs for CXCR1. The experiment was repeated twice with similar results; a representative experiment is shown. (f–g) *Runx1:mCherry;kdrl:GFP* double transgenic embryos were injected with DNA encoding empty vector or *hsp70l:cxcr1* and gene expression was induced at 36 and 48 hpf, followed by time lapse microscopy. (f) Representative still frames showing an HSPC (arrow) entering an endothelial cell pocket ($f_{i\text{-}iii}$), followed by cuddling ($f_{iv\text{-}xvii}$) and finally exit from the endothelial cell pocket (f_{xviii}). Numbers in the bottom left corner of each frame represent hh:mm after fertilization; this track lasted for 8.5 h and produced one mitotic event (f_{vi}, arrowhead). Bar, 20 μm. (g) The time that each tracked HSPC spent cuddled in the endothelial cell pocked is plotted as a percent of the overall track duration within the CHT ($P = 6.28 \times 10^{-7}$, Wilcoxon's rank sum test). $n = 5$ animals, 354 tracked HSPCs for Control and $n = 3$ animals, 114 tracked HSPCs for CXCR1. The experiment was repeated twice with similar results; a representative experiment is shown.

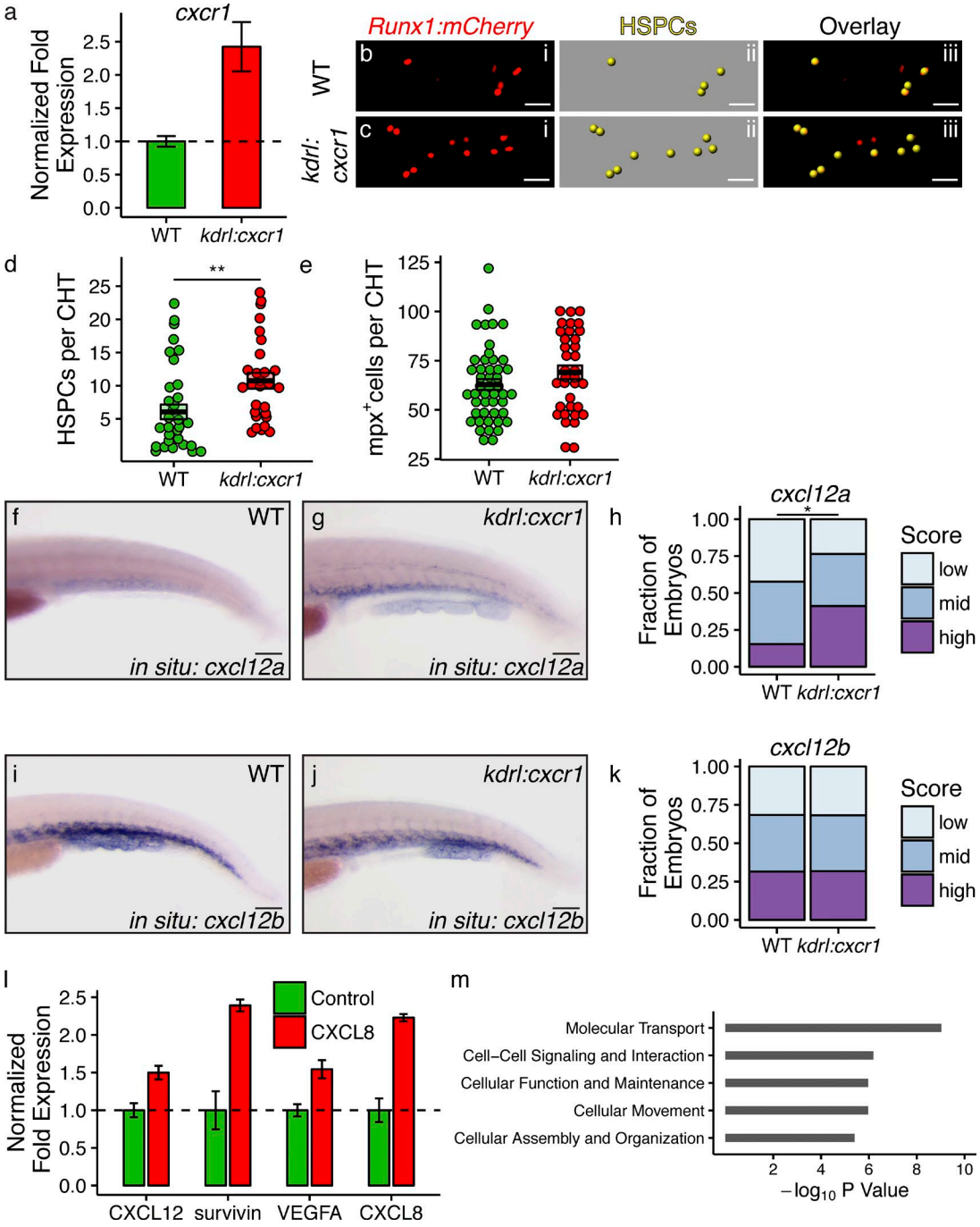

Figure 5. **Cxcl8/cxcr1 signaling in endothelial cells induces gene expression changes favoring HSPC colonization.** (a) *Kdrl:cxcr1;kdrl :mCherry* zebrafish and *kdrl:mCherry* clutchmates (WT) were dissociated at 72 hpf, and mCherry$^+$ endothelial cells were FACS sorted. Quantitative PCR for *cxcr1* is shown. The experiment was repeated three times with similar results. (b–d) *Kdrl:cxcr1;Runx1:mCherry* zebrafish were imaged at 72 hpf for HSPC colonization of the CHT (a and b). Bars, 20 µm. (d) Plot showing increased HSPC colonization in *kdrl:cxcr1* animals (P = 0.001, Wilcoxon's rank sum test; *n* = 35 for WT control; *n* = 28 for *kdrl:cxcr1*) The experiment was repeated twice with similar results; combined results are shown. (e) *Mpx:GFP* (WT) and *kdrl:cxcr1;mpx:GFP* zebrafish were imaged at 72 hpf, and neutrophil numbers in the CHT were quantified (p = NS, Student's *t* test; *n* = 47 for WT control; *n* = 35 for *kdrl:cxcr1*). The experiment was repeated three times with similar results. Combined results are shown. (f–k) *Kdrl:cxcr1* and WT clutchmates were fixed at 72 hpf and WISH was performed for *cxcl12a* (f–h) and *cxcl12b* (i–k). Bar, 100 µm. h and k show the results of blinded semiquantitative scoring of CHT staining for each probe (*cxcl12a:* P = 0.03, Wilcoxon's rank sum test, *n* = 26 for WT control and *n* = 34 for *kdrl:cxcr1*; *cxcl12b*: p = NS, Wilcoxon's rank sum test, *n* = 19 for WT control and *n* = 22 for *kdrl:cxcr1*). The experiment was performed three times with similar results; combined results are shown. (l) HUVECs were serum starved for 12 h, and then treated with 10 ng/ml

with conjoined anterior structures, shared circulation, and morphologically normal bodies and tails. Approximately 70% of all viable parabiotics met these criteria. *Kdrl:GFP* embryos were modified by microinjection of DNA encoding *hsp70l:cxcr1* or empty vector as a control, and were fused to uninjected clutchmates (Fig. 7, a and b). The injected side of each pair was marked by co-injecting fluorescent dextran (Fig. 7, c and d). Gene expression was induced by heat shock at 36 and 48 hpf and CHT volume was measured in both sides of each parabiotic at 72 hpf by fluorescence confocal microscopy followed by 3D digital reconstruction. The fold change in CHT volume (injected:uninjected) is plotted in Fig. 7 e. As expected, when parabiotics were injected with control DNA, the fold change in CHT volume was close to 1 (0.9 ± 0.05-fold change). However, when *hsp70l:cxcr1* was injected, CHT volume was significantly increased on the injected side (1.27 ± 0.11-fold change; P = 0.012, compared with control parabiotics). This increase in the CXCR1 group is in line with what was observed in our heat shock induction experiments in single organisms. These data indicate that *cxcr1* acts locally within the niche and not via circulating cells or other factors that would otherwise have transited to the uninjected side and nullified any difference in CHT volume.

Finally, we created a parabiotic zebrafish system that allowed us to quantify HSPC engraftment in a genetically distinct niche. *Runx1:mCherry* donor zebrafish were fused to *casper* recipient zebrafish that had been injected with DNA encoding either *cxcr1* or GFP under control of the *hsp70l* promoter (Fig. 7 f). In this system, the donor niche is unmodified and donor-derived HSPCs can be detected in both donor and recipient CHTs (Fig. 7, g and h). Gene expression was induced by heat shock at 36 and 48 hpf, parabiotics were imaged at 72 hpf and donor-derived HSPCs colonizing the autologous donor niche and those engrafted in the recipient niche were quantified using unbiased digital image analysis. In control parabiotics expressing GFP within the recipient niche, there was no difference in donor-derived HSPC colonization of the donors and engraftment of the recipients (3.8 ± 1.7 vs. 5.0 ± 1.8 HSPCs per CHT, p = NS, Fig. 7 i). However, when *cxcr1* was overexpressed within the recipient niche, donor-derived HSPC engraftment of the recipient niche was significantly greater than colonization of the autologous donor niche (11.4 ± 2.1 vs. 19.8 ± 3.1 per CHT; P = 0.019; Fig. 7 i). Moreover, this increase was not simply the result of preferential homing, as overexpression of *cxcr1* increased HSPC numbers in both donors and recipients compared with control parabiotics (P = 0.045 for donors and P = 0.007 for recipients, Fig. 7 i). Rather, these data suggest that the action of *cxcr1* within the recipient niche allowed expansion of donor-derived HSPCs, likely by increasing residency time and mitotic rate. This expanded pool of donor cells then freely circulated back to the donor niche. These parabiotic models show that the activity of *cxcr1* is nonautonomous to HSPCs and other circulating cells. Together with the effects seen in the *kdrl:cxcr1* transgenic model, they provide further data in support of a role for *cxcr1* in acting autonomously within the vascular niche to promote HSPC engraftment.

DISCUSSION

HSPC–microenvironment interactions are critical for maintaining the hematopoietic system under steady-state conditions and to allow the organism to respond to systemic stress such as hemorrhage, infection, toxin exposure, chemotherapeutic treatment or radiation damage (Hooper et al., 2009; Ding et al., 2012; Inra et al., 2015). Vertebrate development is characterized by rapid expansion of the hematopoietic system, and thus embryonic hematopoiesis in the zebrafish CHT reflects the biology of hematopoietic regeneration after toxic, inflammatory, or infectious insult (Tamplin et al., 2015). A growing body of literature has made it clear that the microenvironment communicates with HSPCs via proinflammatory cytokine signals in the settings of stress, embryonic or fetal development, and hematologic malignancies (Mirantes et al., 2014; Luis et al., 2016). Here, we have used gain- and loss-of-function experiments in the developing zebrafish to show that signaling via the proinflammatory chemokine receptor, *cxcr1,* enhances HSPC colonization of the sinusoidal endothelial cell niche.

Work from our laboratory has recently shown that an intronic enhancer sequence from the murine *Runx1* gene (*Runx1+23*) marks zebrafish hematopoietic stem cells with long-term repopulating capacity when linked to mCherry or GFP reporter transgenes (Tamplin et al., 2015). This work showed that there are between 4 and 5 phenotypically defined Runx1$^+$ cells within the CHT at this developmental stage, and that ∼1 in 3 of these are long-term HSCs by limiting dilution transplant experiments (Tamplin et al., 2015). The *Runx1* reporter lines were used to demonstrate endothelial cell cuddling of HSPCs within the CHT (Tamplin et al., 2015). We have now used these same lines to begin to uncover the molecular mechanisms by which cuddling and stem cell colonization of the CHT occurs. Visualization of CHT colonization by *Runx1*$^+$ HSPCs in live embryos followed by single cell track analysis demonstrated that *cxcl8/cxcr1* signaling enhances endothelial cell cuddling of HSPCs, prolonging HSPC residency time within the niche and allowing additional mitotic events to occur. Gene expression studies in zebrafish and primary human endothelial cells suggest that *cxcl8/cxcr1* signals in a positive feedback loop, inducing ex-

rhCXCL8 or vehicle control. Quantitative RT-PCR was performed for expression of CXCL12, CXCL8, and survivin and VEGFA. (m) RNA sequencing was performed on HUVEC RNA. IPA analysis identifying the top enriched molecular and cellular functions is shown. The HUVEC experiments were performed with biological duplicates.

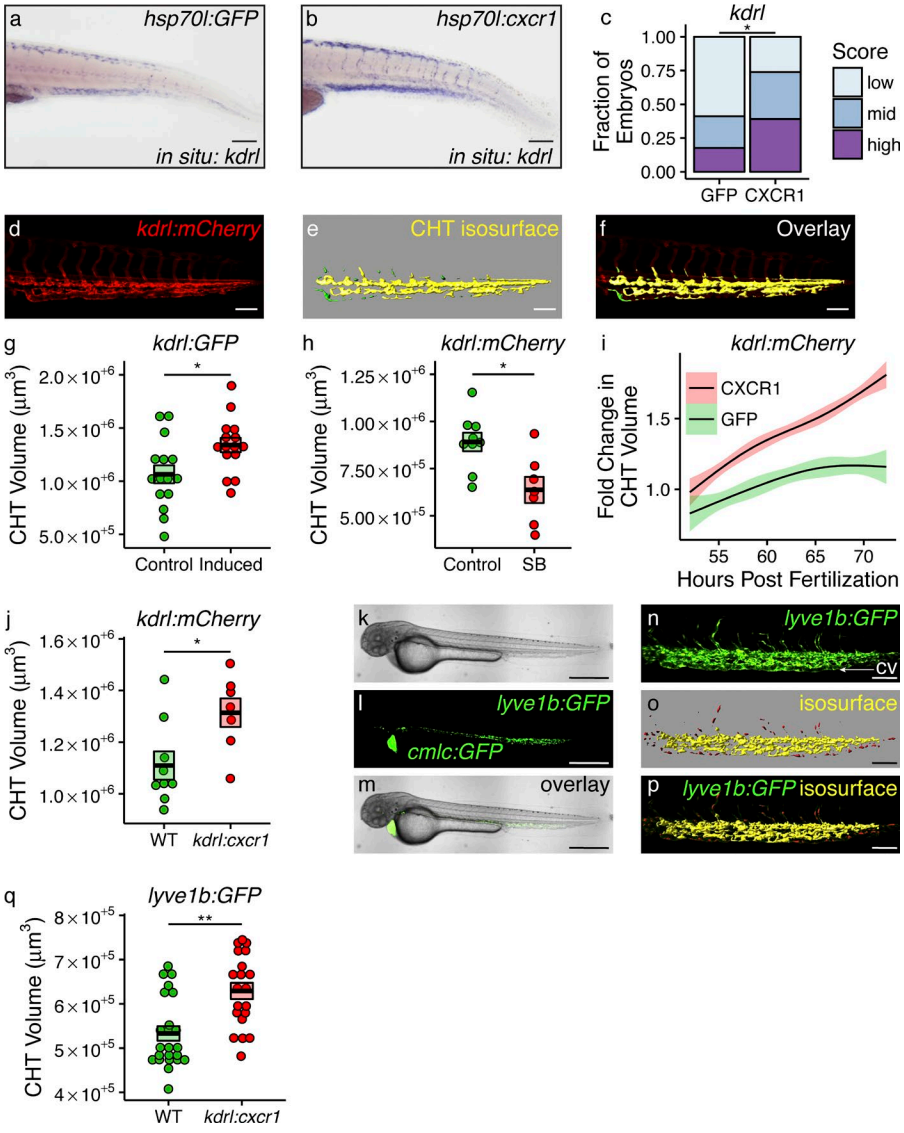

Figure 6. **Cxcr1 signaling alters the structure of the CHT.** (a–c) Overexpression of GFP (control) or *cxcr1* was induced in microinjected zebrafish by heat shock at 36 and 48 hpf. (a and b) Representative WISH images for *kdrl*, marking endothelial cells, at 72 hpf are shown. Bars, 100 µm. (c) Blinded scoring of *kdrl* staining in the CHT (Wilcoxon rank sum test, P = 0.041; *n* = 17 for GFP control; *n* = 23 for *cxcr1*). The experiment was repeated twice with similar results; a representative experiment is shown. (d–f) Isosurface rendering of the CHT using Imaris. A representative *kdrl:mCherry* transgenic fish, imaged at 72 hpf, is shown (d). A three-dimensional isosurface rendering of the CHT and overlay are shown (e and f). Only the yellow portion of the isosurface was included in the volumetric analysis. Bars, 100 µm. (g–j) CHT volume was measured in *kdrl:GFP* or *kdrl:mCherry* reporter zebrafish at 72 hpf. CHT volume is plotted in μm^3. (g) All zebrafish were injected with *hsp70l:cxcr1* DNA and gene expression was induced in one half of the animals by heat shock at 36 and 48 hpf (Wilcoxon rank sum test, P = 0.02, *n* = 15 for uninduced controls and *n* = 15 for heat shock–induced embryos). The experiment was repeated three times with similar results, a representative experiment is shown. (h) *Kdrl:mCherry* transgenic fish were treated with the CXCR1/2 inhibitor SB225002 (SB) or DMSO control from 48 to 72 hpf (Student's *t* test, P = 0.012; *n* = 9 for untreated controls; *n* = 7 for treated embryos). The experiment was repeated twice with similar results; a representative experiment is shown. (i) *Kdrl:mCherry* zebrafish were injected with *hsp70l:cxcr1* DNA or *hsp70l:GFP* as a control followed by heat shock at 36 and 48 hpf. A time series plot showing the relative change in CHT volume from 52 to 72 hpf compared with baseline is shown. Colored bands represent 95% confidence intervals. *n* = 5 for GFP control and *n* = 5 for *hsp70l:cxcr1*. The experiment was repeated twice with similar results; a representative experiment is shown. (j) The CHT volume of *kdrl:mCherry;kdrl:cxcr1* zebrafish and *kdrl:mCherry* (WT) clutchmates is shown (Student's *t* test, P = 0.02; *n* = 9 for WT; *n* = 7 for *kdrl:cxcr1*). The experiment was repeated twice, with similar results. A representative experiment is shown. (k–p) Representative images of a *lyve1b:GFP;kdrl:cxcr1* transgenic are shown. (k–m) Low power views showing expression of the *lyve1b:GFP* reporter transgene predominantly in the CHT. GFP expression in the heart is driven by a secondary marker transgene (*cmlc:GFP*) for *kdrl:cxcr1*. Bars, 500 µm. (n–p) High power views of the CHT in the same embryo. (n) GFP expression in the CHT and caudal vein (CV). (o) Three dimensional isosurface of the *lyve1b:GFP*-expressing tissues. Only the yellow portion of the isosurface is used for quantifying CHT volume. (p) Overlay of the isosurface and *lyve1b:GFP* expression. Bars, 100 µm. (q) The CHT volume of *lyve1b:DsRed* (WT) and *kdrl:cxcr1;lyve1b:DsRed* (*kdrl:cxcr1*) transgenics was measured at 72 hpf as before (P = 0.0006, Wilcoxon rank sum test; *n* = 23 for WT; *n* = 20 for *kdrl:cxcr1*). The experiment was repeated twice with similar results; a representative experiment is shown.

pression of *cxcl12a* in the process and providing a molecular mechanism to promote HSPC retention.

The embryonic zebrafish is unique among vertebrates in that the entire hematopoietic niche can be imaged at fine spatiotemporal resolution. Digital image analysis allowed us to reconstruct the CHT in three dimensions and to quantitate changes in CHT volume in the presence of enhanced *cxcr1* signaling. Though we cannot rule out the possibility that *cxcr1* may act via induction of secondary paracrine factors that act locally within the niche, our experiments using *kdrl:cxcr1* transgenic fish, HUVECs, and parabiotic zebrafish strongly support the notion that *cxcr1* acts directly on the vascular niche, expanding its volume and enhancing HSPC engraftment and proliferation. Based on these data, we

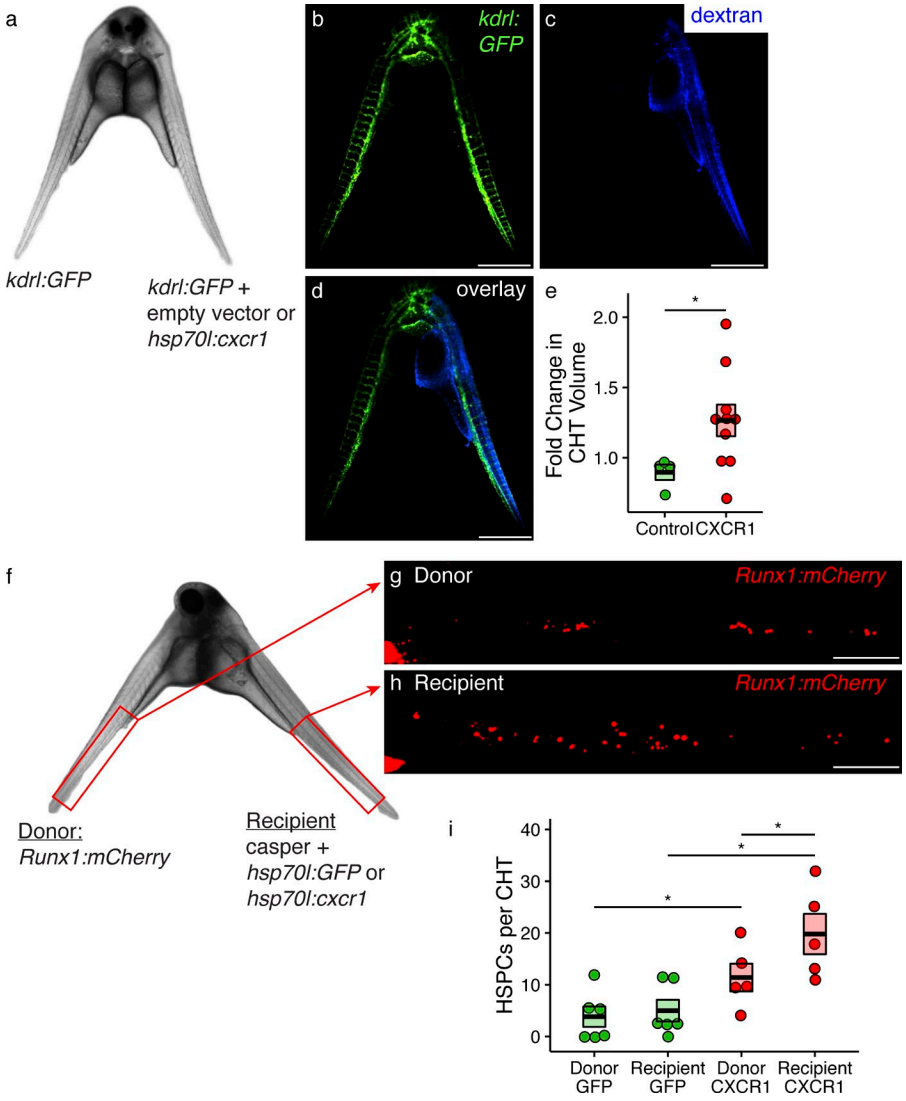

Figure 7. **Cxcr1 acts stem cell nonautonomously in parabiotic zebrafish.** (a–e) Uninjected *kdrl:GFP* embryos were fused to *kdrl:GFP* embryos injected with DNA encoding *hsp70l:cxcr1* or empty vector (Control), and gene expression was induced at 36 and 48 hpf. Fluorescent blue dextran was used to mark the injected halves of each pair. (a–d) Low magnification views showing a representative parabiotic from this experiment in transmitted light (a), green channel (b), blue channel (c), and green/blue overlay. Bars, 500 µm. (e) The fold change in CHT volume (injected:uninjected) is plotted for Control and CXCR1 groups (P = 0.012, Student's *t* test; *n* = 4 for Control; *n* = 10 for CXCR1). The experiment was repeated twice with similar results; combined results are shown. (f–i) In these parabiotic animals, donor halves are *Runx1:mCherry* transgenics and recipient halves are *casper* injected with DNA encoding *hsp70l:GFP* or *hsp70l:cxcr1* followed by heat shock induction at 36 and 48 hpf. (f–h) Representative transmitted light and fluorescence images of these parabiotics. The CHT of the donor and recipient animal is boxed in red and shown in fluorescence in panels g and h. Bars, 100 µm. (i) Expression of *cxcr1* in the recipient niche favored HSPC engraftment there over colonization of the donor autologous niche (red circles, P = 0.019, paired Student's *t* test). There was no difference between donors and recipients in the GFP group (green circles). Overall HSPC numbers were also increased in donors and recipients by recipient expression of *cxcr1* (donor GFP vs. CXCR1, P = 0.045, Student's *t* test; recipient GFP vs. CXCR1, P = 0.007, Student's *t* test). *n* = 6 for GFP control; *n* = 5 for CXCR1. The experiment was repeated twice with similar results; combined results are shown.

propose the following novel mechanism: before the onset of HSPC colonization, the primitive vascular niche of the CHT expresses low levels of *cxcr1* and *cxcl8*. *Cxcl8* is induced within the niche in the presence of local vasoactive lipid mediators such as EET. It is possible that myeloid cells or a subset of HSPCs produce *cxcl8* under some circumstances as even stem and progenitor cells have been shown to be potent cytokine producers (Zhao et al., 2014; Li et al., 2015; Sinclair et al., 2016). *Cxcl8* signals in an autocrine/paracrine fashion via *cxcr1* on endothelial cells, inducing expression of *vegfa* and promoting survival and motility of the sinusoidal endothelial cells within the CHT. *Cxcl12a* is induced, allowing

colonization and maintenance of HSPCs within the niche. *Cxcr1* promotes endothelial cuddling, which allows HSPCs to expand and produce more mature myeloid cells which may also support the niche through *cxcl8* expression. By 5–6 dpf, the kidney marrow has developed and outcompetes the CHT as a favorable HSPC niche. We speculate that the loss of *cxcl8*-producing progenitors and myeloid cells at this time interrupts the proangiogenic positive feedback loop in the CHT and allows the terminal differentiation of the sinusoids into intersegmental veins.

Though *cxcl8/cxcr1* signaling has well defined roles in host defense, angiogenesis, and inflammation, this pathway is only beginning to be understood as an important factor in hematopoiesis (Cacalano et al., 1994; Terashima et al., 1998; Waugh and Wilson, 2008; Deng et al., 2013; Zhang et al., 2015). We have recently found that loss of *cxcl8* signaling leads to a lower rate of endothelial–hematopoietic transformation (EHT) and reduced HSC numbers in the AGM (Bertrand et al., 2010; Kissa and Herbomel, 2010; Jing et al., 2015). This role for *cxcl8* in the specification of HSCs from hemogenic endothelium is in accordance with other work demonstrating that TNF, IFN-γ, PGE_2, EET, TLR agonists, and other proinflammatory mediators are important for the earliest phase of definitive hematopoiesis (North et al., 2007; Espín-Palazón et al., 2014; Sawamiphak et al., 2014; He et al., 2015; Li et al., 2015).

Beyond HSC specification, *cxcl8* and other chemokines have been implicated in the complex interplay between HSPCs and mature myeloid cells in the process of mobilization from the niche. In an early study, a single dose of recombinant human CXCL8 was found to rapidly mobilize HSPCs in mice (Laterveer et al., 1995). Extensive work by the Pelus laboratory has compared the mobilization characteristics of several members of the CXC family of chemokines and has highlighted the importance of CXCL2 (Gro-β) signaling via CXCR2 in this process (Pelus et al., 2002). In these studies, stem cell mobilization appears to be dependent on MMP-9 and CXCR2 expression by neutrophils (Cacalano et al., 1994; Pelus et al., 2004; Pelus and Fukuda, 2006). In addition, a recent study has shown that $CXCR2^{-/-}$ mice have impaired vascular regeneration in the marrow after lethal irradiation (Hale et al., 2015). Nevertheless, placing CXCL8/CXCR1 precisely within this conceptual framework has been difficult because mice lack a close ortholog of CXCL8, its absence likely complemented by CXCL1 (Gro-α/KC) and CXCL2 (Gro-β/MIP-2; Lee et al., 1995; Wang et al., 1997).

In zebrafish, the CXC–chemokine system is complicated by an ancestral genome amplification event that produced three *cxcl8* genes, located on chromosomes 1, 7, and 17 (van der Aa et al., 2010). Zebrafish *cxcl8* is expressed in leukocytes, though the different contributions of each *cxcl8* locus remain poorly understood (Oehlers et al., 2010). *Cxcr1* and *cxcr2* are broadly expressed in leukocytes, vasculature, the developing gut, and elsewhere (Oehlers et al., 2010; Deng et al., 2013). In a zebrafish model of pseudomonas infection, *cxcr2* knockdown, but not *cxcr1* knockdown, reduced neutrophil chemotaxis to *cxcl8* and leukotriene B4 and impaired localization at the site of infection, indicating that *cxcl8/cxcr2* is the critical pathway in response to infection. Intriguingly, the same study noted that whereas *cxcr1* knockdown did not alter neutrophil responses to infection, it did substantially reduce the number of neutrophils present in the CHT at 72 hpf (whereas *cxcr2* knockdown had no effect in the CHT), suggesting that *cxcr1* may be involved in myeloid development (Deng et al., 2013). We now directly show that *cxcr1* is an important mediator of HSPC engraftment within the vascular niche, whereas *cxcr2* may have little or no role in this process.

Understanding the interactions between HSPCs and the vascular niche in the setting of vertebrate development has shed light on how the hematopoietic system responds to stress conditions. Additional mechanistic studies in animal models of normal and stress hematopoiesis will be necessary to fully understand the role of CXCL8, CXCR1, and CXCR2 in hematopoietic recovery after administration of chemotherapy, engraftment after HSCT, and in the development of hematologic malignancies and myeloproliferative disorders. However, one can speculate that modulating CXCL8/CXCR1 signaling in these patients might aid in favorably remodeling the niche to promote the recovery of normal hematopoiesis.

MATERIALS AND METHODS

Zebrafish

Wild-type AB, *casper*, and transgenic lines *Runx1:GFP*, *Runx1:mCherry* (Tamplin et al., 2015), *kdrl:GFP* (Jin et al., 2005), *kdrl:mCherry* (Chi et al., 2008), *lyve1b:GFP* (Okuda et al., 2012), *sclβ:GFP* (Zhen et al., 2013), and *kdrl:cxcr1* were used in this study. Embryos were used up to 84 hpf. $Cxcl8^{-/-}$ fish were generously provided by A. Huttenlocher. All animals were housed at Boston Children's Hospital and were maintained according to institutional animal care and use committee protocols.

Flow cytometry

Zebrafish embryos were manually dissociated in PBS containing collagenase (Liberase; Sigma-Aldrich) at 72 hpf. Adult zebrafish were euthanized by tricaine overdose and ice water immersion, and kidney marrow was harvested. Single-cell suspensions were made using a 40-µm filter and indicated cell populations were sorted by FACS using a FACSAria machine (BD).

Candidate gene selection

Total RNA was purified from flow-sorted cells, and gene expression profiling was performed by microarray analysis (Zebrafish 1.0 ST Array; Affymetrix) as previously described (Tamplin et al., 2015). Gene sets were created by searching the NCBI Gene database for the categories of extracellular and secreted molecules listed in Table S1. Gene set enrichment analysis was performed using adult and embryonic gene expression datasets with three biological replicates for endothelial cells and HSPCs. GSEA v2.2.0 software was used for

the analysis. Entrez IDs were used to identify genes in the gene sets and gene expression data. Between 44 and 90% of the genes in each gene set were included in the expression datasets. Leading edge subsets of each gene set were identified for the adult and embryonic data and overlap was identified using Venny 2.0.

Data availability

Microarray and RNaseq data are available from the Gene Expression Omnibus under accession nos. GSE56015 and GSE92543.

Nomenclature

There is variability in the literature and informatics databases regarding the nomenclature for the zebrafish *cxcr1* and *cxcr2* genes. We have used the identifications suggested by Deng et al., 2013 for *cxcr1* (Entrez ID: 797181; Ensembl gene: ENSDARG00000052088) and *cxcr2* (Entrez ID: 796724; Ensembl gene: ENSDARG00000054975).

Transgenesis

Candidate zebrafish coding sequences were amplified from kidney marrow total RNA using the Superscript III RT kit (Thermo Fisher Scientific) and gene-specific primers. PCR products were cloned into the pentr SD Topo middle entry vector (Invitrogen), and then into Tol2-based expression vectors via Gateway reaction (Kwan et al., 2007). *Hsp70l* and *kdrl* promoters were used as 5′ sequences (Adám et al., 2000; Jin et al., 2005). Tol2 expression vectors (20 pg per construct) were microinjected into the cell of zebrafish zygotes. *Hsp70l:GFP* (5 pg) was co-injected to mark successfully injected embryos with high mosaicism. Tol2 mRNA (200 pg) was co-injected to enhance genomic integration of the constructs. Viable embryos were selected at 24 hpf.

Heat shock induction of gene expression

Viable embryos were transferred to 96-well PCR plates at indicated time points in 100 µl embryo water. Heat shock was performed in a standard PCR thermal cycler. Embryos were incubated at 40°C for 30 min before being returned to the standard incubator (28°C). A second heat shock was performed 12 h later, and animals were removed from the plates by gently flushing each well with embryo water.

Drug treatment

Zebrafish embryos were treated by adding SB225002 (0.5 µM) or dimethyl PGE_2 (10 µM) directly to the fish water at the indicated time points (Cayman Chemicals). An equal volume of DMSO was added to the fish water for control groups to serve as a negative control.

In situ hybridization

Zebrafish embryos were euthanized by tricaine overdose and fixed in 4% PFA before in situ hybridization for *runx1* was performed and *c-myb*, *cxcl12a*, *cxcl12b*, or *kdrl* mRNA using standard techniques (Thisse and Thisse, 2008). For scoring, groups of 10–20 embryos were deidentified and suspended in glycerol before performing a semiquantitative assessment of the intensity of specific staining in the CHT region. Zebrafish groups were unblinded and scores compared using the Wilcoxon rank sum test (R v3.2.2).

Zebrafish parabiosis

Parabiotic zebrafish were made according to published protocols (Demy et al., 2013; Hagedorn et al., 2016). In brief, zebrafish embryos were fused at the 1,000-cell stage by embedding in methylcellulose and covering in high-calcium Ringer's solution containing penicillin and streptomycin. Approximately 70% of such animals developed with fused heads, morphologically normal tails, and shared circulation. Successfully joined parabiotic animals underwent heat shock induction of gene expression as described.

Confocal microscopy

Zebrafish embryos and parabiotics were anesthetized with tricaine and embedded in 1.2% agarose on MatTek glass-bottom 6-well plates using standard techniques (Westerfield, 2007). Images were acquired using a Yokogawa spinning disk confocal and Nikon inverted Ti microscope. A Nikon 20× air Plan-Apo differential interference contrast NA 0.75 objective was used. Images were acquired with Andor iXon x3 EMC CD cameras and NIS Elements software. Confocal z-stacks were acquired at 2 µm intervals. Time lapse video frames were acquired every 10–30 min, depending on acquisition time, using an automated stage.

Digital image analysis

All image analysis was performed using Imaris software (Bitplane) as described in detail in the Results section.

Cell culture

Primary zebrafish endothelial cells were treated with EET (5 µM) or DMSO control for 30 min at room temperature before lysis and RNA purification (Li et al., 2015). Primary HUVECs were cultured in supplemented M200 medium containing hEGF, hydrocortisone, hFGF, VEGF, R3-IGF-1, ascorbic acid, heparin, and fetal bovine serum (Gibco). Cells were grown in a humidified 5% CO_2 atmosphere at 37°C. Cells were starved in unsupplemented medium for 12 h before addition of recombinant human CXCL8 (R&D Systems) at a final concentration of 10 ng/ml or an equal volume of vehicle control (water). Cells were harvested after 6 h of treatment, and RNA was purified using the RNeasy Plus Mini kit (QIAGEN). For protein expression experiments, HUVEC culture supernatants were harvested and filtered before analysis by ELISA. Human VEGF and CXCL12 ELISA kits were purchased from Abcam and used according to the manufacturer's instructions.

Quantitative PCR

Total RNA was purified from zebrafish endothelial cells, HSPCs, and HUVECs using the RNeasy Plus Mini kit (QIAGEN). Complementary DNA was reverse transcribed using the SuperScript III RT kit (Thermo Fisher Scientific) and a mixture of poly-A and random hexamer primers. Quantitative PCR was performed using SSOFast Supermix with EvaGreen (Bio-Rad Laboratories) and a Bio-Rad thermal cycler. The following primer sequences were used in the study: zf-18s: 5′-TCGCTAGTTGGCATC GTTTATG-3′ (forward), 5′-CGGAGGTTCGAAGAC GATCA-3′ (reverse); zf-cxcl8: 5′-TCATTGAAGGAATGA GCTTGAGAG-3′ (forward), 5′-CCAGTTGTCATCAAG GTGGC-3′ (reverse); zf-cxcr1: 5′-GTGATCGTACGC GCTATGGA-3′ (forward), 5′-ATTCGGGTTGCTAAT CGCCA-3′ (reverse) ; hs-CXCL12: 5′-ACATGGCTT TCGAAGAATCG-3′ (forward), 5′-GCTGGTCCTCGT GCTGAC-3′ (reverse); hs-survivin: 5′-TTGGTGAATTTT TGAAACTGGA-3′ (forward), 5′-CTTTCTCCGCAG TTTCCTCA-3′ (reverse); hs-VEGFa: 5′-AGGGCAGAA TCATCACGAAGT-3′ (forward), 5′-AGGGTCTCGATT GGATGGCA-3′ (reverse) ; hs-CXCL8 5′-AAATTTGGG GTGGAAAGGTT-3′ (forward), 5′-TCCTGATTTCTG CAGCTCTGT-3′ (reverse).

RNA sequencing

For the HUVEC RNA-seq, ribosomal RNA was depleted from total RNA using the Ribo-Zero kit (Epicentre) according to the manufacturer's instructions. Sequencing libraries were constructed using the NEBNext Ultra kit for Illumina (New England Biolabs). For zebrafish endothelial cell RNA-seq, cells were lysed in TRIzol LS and total RNA was extracted by phenol-chloroform extraction and isopropanol precipitation. Messenger RNA selection and first-strand cDNA synthesis was performed using the SMARTer Universal Low Input RNA kit (Takara Bio Inc.). Libraries were synthesized using the Low Input Library Prep kit for Illumina (Takara Bio Inc.). All libraries were sequenced on an Hi-Seq 2500 instrument (Illumina).

Statistical analysis

For the GSEA experiments, enrichment scores and P-values were calculated by the GSEA software package (Subramanian et al., 2005). The remainder of the statistical analyses were performed and data were plotted using R v3.2.2. No statistical method was used to predetermine sample size. Embryos were randomly selected for experimental and control groups before DNA injection. All animals with normal morphology, expected levels of reporter transgene expression, and normal circulation were included in the analyses. Sample variations were compared using the Kolmogorov-Smirnov test. HSPC numbers and CHT volume were then compared using the two-sided Student's *t* test or the Wilcoxon rank sum test, depending on the sample distributions. In situ hybridization data were compared using the Wilcoxon rank sum test. In all tests, $P < 0.05$ was considered to be statistically significant. Mean ± SEM is reported unless indicated otherwise.

Online supplemental material

Fig. S1 shows the bioinformatic workflow used to identify differentially regulated genes between endothelial cells and HSCs and to select candidate genes for the gain-of-function screen. Fig. S2 provides an example of the degree of global overexpression achieved in our gain-of-function experiments. Video 1 shows a representative HSC-endothelial cell cuddling event. Tables S1–S6, available as Excel files, identify the gene sets, component genes, and results of GSEA.

ACKNOWLEDGMENTS

This work was supported by National Institutes of Health R01HL04880, P01HL032262, P30DK049216, R01DK53298, U01HL10001, R24DK092760 (L.I.Z.) and postdoctoral awards from Alex's Lemonade Stand Foundation, the Cancer Research Institute, and the Conquer Cancer Foundation of ASCO (B.W.B.). L.I.Z. is a founder and stock holder of Fate Therapeutics, Marauder Therapeutics, and Scholar Rock. The authors declare no competing financial interests.

Author contributions: Conceptualization, B.W. Blaser and L.I. Zon; Methodology, B.W. Blaser and L.I. Zon; Investigation, B.W. Blaser, J.L. Moore, E.J. Hagedorn, B. Li, V.B., O.T., R. Riquelme, A. Lichtig, S. Yang, and Y. Zhou; Writing (original draft), B.W. Blaser; Writing (Review) & Editing, B.W. Blaser and L.I. Zon; Funding Acquisition, B.W. Blaser and L.I. Zon; Resources, L.I. Zon; Supervision, L.I. Zon.

Submitted: 25 September 2016
Revised: 28 December 2016
Accepted: 10 February 2017

REFERENCES

Adám, A., R. Bártfai, Z. Lele, P.H. Krone, and L. Orbán. 2000. Heat-inducible expression of a reporter gene detected by transient assay in zebrafish. *Exp. Cell Res.* 256:282–290. http://dx.doi.org/10.1006/excr.2000.4805

Ara, T., K. Tokoyoda, T. Sugiyama, T. Egawa, K. Kawabata, and T. Nagasawa. 2003. Long-term hematopoietic stem cells require stromal cell-derived factor-1 for colonizing bone marrow during ontogeny. *Immunity.* 19:257–267. http://dx.doi.org/10.1016/S1074-7613(03)00201-2

Bertrand, J.Y., N.C. Chi, B. Santoso, S. Teng, D.Y.R. Stainier, and D. Traver. 2010. Haematopoietic stem cells derive directly from aortic endothelium during development. *Nature.* 464:108–111. http://dx.doi.org/10.1038/nature08738

Butler, J.M., D.J. Nolan, E.L. Vertes, B. Varnum-Finney, H. Kobayashi, A.T. Hooper, M. Seandel, K. Shido, I.A. White, M. Kobayashi, et al. 2010. Endothelial cells are essential for the self-renewal and repopulation of Notch-dependent hematopoietic stem cells. *Cell Stem Cell.* 6:251–264. http://dx.doi.org/10.1016/j.stem.2010.02.001

Cacalano, G., J. Lee, K. Kikly, A.M. Ryan, S. Pitts-Meek, B. Hultgren, W.I. Wood, and M.W. Moore. 1994. Neutrophil and B cell expansion in mice that lack the murine IL-8 receptor homolog. *Science.* 265:682–684. http://dx.doi.org/10.1126/science.8036519

Chen, A.T., and L.I. Zon. 2009. Zebrafish blood stem cells. *J. Cell. Biochem.* 108:35–42. http://dx.doi.org/10.1002/jcb.22251

Chi, N.C., R.M. Shaw, S. De Val, G. Kang, L.Y. Jan, B.L. Black, and D.Y.R. Stainier. 2008. Foxn4 directly regulates tbx2b expression and atrioventricular canal formation. *Genes Dev.* 22:734–739. http://dx.doi.org/10.1101/gad.1629408

Demy, D.L., Z. Ranta, J.-M. Giorgi, M. Gonzalez, P. Herbomel, and K. Kissa. 2013. Generating parabiotic zebrafish embryos for cell migration and homing studies. *Nat. Methods.* 10:256–258. http://dx.doi.org/10.1038/nmeth.2362

Deng, Q., M. Sarris, D.A. Bennin, J.M. Green, P. Herbomel, and A. Huttenlocher. 2013. Localized bacterial infection induces systemic activation of neutrophils through Cxcr2 signaling in zebrafish. *J. Leukoc. Biol.* 93:761–769. http://dx.doi.org/10.1189/jlb.1012534

Ding, L., and S.J. Morrison. 2013. Haematopoietic stem cells and early lymphoid progenitors occupy distinct bone marrow niches. *Nature.* 495:231–235. http://dx.doi.org/10.1038/nature11885

Ding, L., T.L. Saunders, G. Enikolopov, and S.J. Morrison. 2012. Endothelial and perivascular cells maintain haematopoietic stem cells. *Nature.* 481:457–462. http://dx.doi.org/10.1038/nature10783

Espín-Palazón, R., D.L. Stachura, C.A. Campbell, D. García-Moreno, N. Del Cid, A.D. Kim, S. Candel, J. Meseguer, V. Mulero, and D. Traver. 2014. Proinflammatory signaling regulates hematopoietic stem cell emergence. *Cell.* 159:1070–1085. http://dx.doi.org/10.1016/j.cell.2014.10.031

Fernandez, L., S. Rodriguez, H. Huang, A. Chora, J. Fernandes, C. Mumaw, E. Cruz, K. Pollok, F. Cristina, J.E. Price, et al. 2008. Tumor necrosis factor-alpha and endothelial cells modulate Notch signaling in the bone marrow microenvironment during inflammation. *Exp. Hematol.* 36:545–558. http://dx.doi.org/10.1016/j.exphem.2007.12.012

Flores, M.V., C.J. Hall, K.E. Crosier, and P.S. Crosier. 2010. Visualization of embryonic lymphangiogenesis advances the use of the zebrafish model for research in cancer and lymphatic pathologies. *Dev. Dyn.* 239:2128–2135. http://dx.doi.org/10.1002/dvdy.22328

Hagedorn, E.J., J.L. Cillis, C.R. Curley, T.C. Patch, B. Li, B.W. Blaser, R. Riquelme, L.I. Zon, and D.I. Shah. 2016. Generation of parabiotic zebrafish embryos by surgical fusion of developing blastulae. *J. Vis. Exp.* e54168. http://dx.doi.org/10.3791/54168

Hale, S.J.M., A.B.H. Hale, Y. Zhang, D. Sweeney, N. Fisher, M. van der Garde, R. Grabowska, E. Pepperell, K. Channon, E. Martin-Rendon, and S.M. Watt. 2015. CXCR2 modulates bone marrow vascular repair and haematopoietic recovery post-transplant. *Br. J. Haematol.* 169:552–564. http://dx.doi.org/10.1111/bjh.13335

Halloran, M.C., M. Sato-Maeda, J.T. Warren, F. Su, Z. Lele, P.H. Krone, J.Y. Kuwada, and W. Shoji. 2000. Laser-induced gene expression in specific cells of transgenic zebrafish. *Development.* 127:1953–1960.

He, Q., C. Zhang, L. Wang, P. Zhang, D. Ma, J. Lv, and F. Liu. 2015. Inflammatory signaling regulates hematopoietic stem and progenitor cell emergence in vertebrates. *Blood.* 125:1098–1106. http://dx.doi.org/10.1182/blood-2014-09-601542

Hooper, A.T., J.M. Butler, D.J. Nolan, A. Kranz, K. Iida, M. Kobayashi, H.-G. Kopp, K. Shido, I. Petit, K. Yanger, et al. 2009. Engraftment and reconstitution of hematopoiesis is dependent on VEGFR2-mediated regeneration of sinusoidal endothelial cells. *Cell Stem Cell.* 4:263–274. http://dx.doi.org/10.1016/j.stem.2009.01.006

Inra, C.N., B.O. Zhou, M. Acar, M.M. Murphy, J. Richardson, Z. Zhao, and S.J. Morrison. 2015. A perisinusoidal niche for extramedullary haematopoiesis in the spleen. *Nature.* 527:466–471. http://dx.doi.org/10.1038/nature15530

Jin, S.-W., D. Beis, T. Mitchell, J.-N. Chen, and D.Y.R. Stainier. 2005. Cellular and molecular analyses of vascular tube and lumen formation in zebrafish. *Development.* 132:5199–5209. http://dx.doi.org/10.1242/dev.02087

Jing, L., O.J. Tamplin, M.J. Chen, Q. Deng, S. Patterson, P.G. Kim, E.M. Durand, A. McNeil, J.M. Green, S. Matsuura, et al. 2015. Adenosine signaling promotes hematopoietic stem and progenitor cell emergence. *J. Exp. Med.* 212:649–663. http://dx.doi.org/10.1084/jem.20141528

Kissa, K., and P. Herbomel. 2010. Blood stem cells emerge from aortic endothelium by a novel type of cell transition. *Nature.* 464:112–115. http://dx.doi.org/10.1038/nature08761

Kobayashi, H., J.M. Butler, R. O'Donnell, M. Kobayashi, B.-S. Ding, B. Bonner, V.K. Chiu, D.J. Nolan, K. Shido, L. Benjamin, and S. Rafii. 2010. Angiocrine factors from Akt-activated endothelial cells balance self-renewal and differentiation of haematopoietic stem cells. *Nat. Cell Biol.* 12:1046–1056. http://dx.doi.org/10.1038/ncb2108

Krause, D.S., and D.T. Scadden. 2012. Deconstructing the complexity of a microenvironmental niche. *Cell.* 149:16–17. http://dx.doi.org/10.1016/j.cell.2012.03.005

Kunisaki, Y., I. Bruns, C. Scheiermann, J. Ahmed, S. Pinho, D. Zhang, T. Mizoguchi, Q. Wei, D. Lucas, K. Ito, et al. 2013. Arteriolar niches maintain haematopoietic stem cell quiescence. *Nature.* 502:637–643. http://dx.doi.org/10.1038/nature12612

Kwan, K.M., E. Fujimoto, C. Grabher, B.D. Mangum, M.E. Hardy, D.S. Campbell, J.M. Parant, H.J. Yost, J.P. Kanki, and C.-B. Chien. 2007. The Tol2kit: a multisite gateway-based construction kit for Tol2 transposon transgenesis constructs. *Dev. Dyn.* 236:3088–3099. http://dx.doi.org/10.1002/dvdy.21343

Laterveer, L., I.J. Lindley, M.S. Hamilton, R. Willemze, and W.E. Fibbe. 1995. Interleukin-8 induces rapid mobilization of hematopoietic stem cells with radioprotective capacity and long-term myelolymphoid repopulating ability. *Blood.* 85:2269–2275.

Lee, J., G. Cacalano, T. Camerato, K. Toy, M.W. Moore, and W.I. Wood. 1995. Chemokine binding and activities mediated by the mouse IL-8 receptor. *J. Immunol.* 155:2158–2164.

Li, A., S. Dubey, M.L. Varney, B.J. Dave, and R.K. Singh. 2003. IL-8 directly enhanced endothelial cell survival, proliferation, and matrix metalloproteinases production and regulated angiogenesis. *J. Immunol.* 170:3369–3376. http://dx.doi.org/10.4049/jimmunol.170.6.3369

Li, P., J.L. Lahvic, V. Binder, E.K. Pugach, E.B. Riley, O.J. Tamplin, D. Panigrahy, T.V. Bowman, F.G. Barrett, G.C. Heffner, et al. 2015. Epoxyeicosatrienoic acids enhance embryonic haematopoiesis and adult marrow engraftment. *Nature.* 523:468–471. http://dx.doi.org/10.1038/nature14569

Luis, T.C., C.S. Tremblay, M.G. Manz, T.E. North, K.Y. King, and G.A. Challen. 2016. Inflammatory signals in HSPC development and homeostasis: Too much of a good thing? *Exp. Hematol.* 44:908–912. http://dx.doi.org/10.1016/j.exphem.2016.06.254

Mahony, C.B., R.J. Fish, C. Pasche, and J.Y. Bertrand. 2016. tfec controls the hematopoietic stem cell vascular niche during zebrafish embryogenesis. *Blood.* 128:1336–1345. http://dx.doi.org/10.1182/blood-2016-04-710137

Mirantes, C., E. Passegué, and E.M. Pietras. 2014. Pro-inflammatory cytokines: emerging players regulating HSC function in normal and diseased hematopoiesis. *Exp. Cell Res.* 329:248–254. http://dx.doi.org/10.1016/j.yexcr.2014.08.017

Morrison, S.J., and D.T. Scadden. 2014. The bone marrow niche for haematopoietic stem cells. *Nature.* 505:327–334. http://dx.doi.org/10.1038/nature12984

Murayama, E., K. Kissa, A. Zapata, E. Mordelet, V. Briolat, H.-F. Lin, R.I. Handin, and P. Herbomel. 2006. Tracing hematopoietic precursor migration to successive hematopoietic organs during zebrafish development. *Immunity.* 25:963–975. http://dx.doi.org/10.1016/j.immuni.2006.10.015

Murayama, E., M. Sarris, M. Redd, D. Le Guyader, C. Vivier, W. Horsley, N. Trede, and P. Herbomel. 2015. NACA deficiency reveals the crucial role of somite-derived stromal cells in haematopoietic niche formation. *Nat. Commun.* 6:8375. http://dx.doi.org/10.1038/ncomms9375

Nagasawa, T., S. Hirota, K. Tachibana, N. Takakura, S. Nishikawa, Y. Kitamura, N. Yoshida, H. Kikutani, and T. Kishimoto. 1996. Defects of B-cell lymphopoiesis and bone-marrow myelopoiesis in mice lacking the CXC chemokine PBSF/SDF-1. *Nature.* 382:635–638. http://dx.doi.org/10.1038/382635a0

Nguyen, P.D., G.E. Hollway, C. Sonntag, L.B. Miles, T.E. Hall, S. Berger, K.J. Fernandez, D.B. Gurevich, N.J. Cole, S. Alaei, et al. 2014. Haematopoietic

stem cell induction by somite-derived endothelial cells controlled by meox1. *Nature.* 512:314–318. http://dx.doi.org/10.1038/nature13678

North, T.E., W. Goessling, C.R. Walkley, C. Lengerke, K.R. Kopani, A.M. Lord, G.J. Weber, T.V. Bowman, I.-H. Jang, T. Grosser, et al. 2007. Prostaglandin E2 regulates vertebrate haematopoietic stem cell homeostasis. *Nature.* 447:1007–1011. http://dx.doi.org/10.1038/nature05883

Oehlers, S.H.B., M.V. Flores, C.J. Hall, R. O'Toole, S. Swift, K.E. Crosier, and P.S. Crosier. 2010. Expression of zebrafish cxcl8 (interleukin-8) and its receptors during development and in response to immune stimulation. *Dev. Comp. Immunol.* 34:352–359. http://dx.doi.org/10.1016/j.dci.2009.11.007

Okuda, K.S., J.W. Astin, J.P. Misa, M.V. Flores, K.E. Crosier, and P.S. Crosier. 2012. lyve1 expression reveals novel lymphatic vessels and new mechanisms for lymphatic vessel development in zebrafish. *Development.* 139:2381–2391. http://dx.doi.org/10.1242/dev.077701

Pelus, L.M., and S. Fukuda. 2006. Peripheral blood stem cell mobilization: the CXCR2 ligand GRObeta rapidly mobilizes hematopoietic stem cells with enhanced engraftment properties. *Exp. Hematol.* 34:1010–1020. http://dx.doi.org/10.1016/j.exphem.2006.04.004

Pelus, L.M., D. Horowitz, S.C. Cooper, and A.G. King. 2002. Peripheral blood stem cell mobilization. A role for CXC chemokines. *Crit. Rev. Oncol. Hematol.* 43:257–275. http://dx.doi.org/10.1016/S1040-8428(01)00202-5

Pelus, L.M., H. Bian, A.G. King, and S. Fukuda. 2004. Neutrophil-derived MMP-9 mediates synergistic mobilization of hematopoietic stem and progenitor cells by the combination of G-CSF and the chemokines GRObeta/CXCL2 and GRObetaT/CXCL2delta4. *Blood.* 103:110–119. http://dx.doi.org/10.1182/blood-2003-04-1115

Sawamiphak, S., Z. Kontarakis, and D.Y.R. Stainier. 2014. Interferon gamma signaling positively regulates hematopoietic stem cell emergence. *Dev. Cell.* 31:640–653. http://dx.doi.org/10.1016/j.devcel.2014.11.007

Sinclair, A., L. Park, M. Shah, M. Drotar, S. Calaminus, L.E.M. Hopcroft, R. Kinstrie, A.V. Guitart, K. Dunn, S.A. Abraham, et al. 2016. CXCR2 and CXCL4 regulate survival and self-renewal of hematopoietic stem/progenitor cells. *Blood.* 128:371–383. http://dx.doi.org/10.1182/blood-2015-08-661785

Subramanian, A., P. Tamayo, V.K. Mootha, S. Mukherjee, B.L. Ebert, M.A. Gillette, A. Paulovich, S.L. Pomeroy, T.R. Golub, E.S. Lander, and J.P. Mesirov. 2005. Gene set enrichment analysis: a knowledge-based approach for interpreting genome-wide expression profiles. *Proc. Natl. Acad. Sci. USA.* 102:15545–15550. http://dx.doi.org/10.1073/pnas.0506580102

Sugiyama, T., H. Kohara, M. Noda, and T. Nagasawa. 2006. Maintenance of the hematopoietic stem cell pool by CXCL12-CXCR4 chemokine signaling in bone marrow stromal cell niches. *Immunity.* 25:977–988. http://dx.doi.org/10.1016/j.immuni.2006.10.016

Tamplin, O.J., E.M. Durand, L.A. Carr, S.J. Childs, E.J. Hagedorn, P. Li, A.D. Yzaguirre, N.A. Speck, and L.I. Zon. 2015. Hematopoietic stem cell arrival triggers dynamic remodeling of the perivascular niche. *Cell.* 160:241–252. http://dx.doi.org/10.1016/j.cell.2014.12.032

Terashima, T., D. English, J.C. Hogg, and S.F. van Eeden. 1998. Release of polymorphonuclear leukocytes from the bone marrow by interleukin-8. *Blood.* 92:1062–1069.

Thisse, C., and B. Thisse. 2008. High-resolution in situ hybridization to whole-mount zebrafish embryos. *Nat. Protoc.* 3:59–69. http://dx.doi.org/10.1038/nprot.2007.514

van der Aa, L.M., M. Chadzinska, E. Tijhaar, P. Boudinot, and B.M.L. Verburg-van Kemenade. 2010. CXCL8 chemokines in teleost fish: two lineages with distinct expression profiles during early phases of inflammation. *PLoS One.* 5:e12384. http://dx.doi.org/10.1371/journal.pone.0012384

Wang, J., N. Mukaida, Y. Zhang, T. Ito, S. Nakao, and K. Matsushima. 1997. Enhanced mobilization of hematopoietic progenitor cells by mouse MIP-2 and granulocyte colony-stimulating factor in mice. *J. Leukoc. Biol.* 62:503–509.

Waugh, D.J.J., and C. Wilson. 2008. The interleukin-8 pathway in cancer. *Clin. Cancer Res.* 14:6735–6741. http://dx.doi.org/10.1158/1078-0432.CCR-07-4843

Westerfield, M. 2007. The Zebrafish Book: A Guide for the Laboratory Use of Zebrafish (Danio Rerio). M. Westerfield

Zhang, B., L. Shi, S. Lu, X. Sun, Y. Liu, H. Li, X. Wang, C. Zhao, H. Zhang, and Y. Wang. 2015. Autocrine IL-8 promotes F-actin polymerization and mediate mesenchymal transition via ELMO1-NF-κB-Snail signaling in glioma. *Cancer Biol. Ther.* 16:898–911. http://dx.doi.org/10.1080/15384047.2015.1028702

Zhang, Y., H. Jin, L. Li, F.X.-F. Qin, and Z. Wen. 2011. cMyb regulates hematopoietic stem/progenitor cell mobilization during zebrafish hematopoiesis. *Blood.* 118:4093–4101. http://dx.doi.org/10.1182/blood-2011-03-342501

Zhao, J.L., C. Ma, R.M. O'Connell, A. Mehta, R. DiLoreto, J.R. Heath, and D. Baltimore. 2014. Conversion of danger signals into cytokine signals by hematopoietic stem and progenitor cells for regulation of stress-induced hematopoiesis. *Cell Stem Cell.* 14:445–459. http://dx.doi.org/10.1016/j.stem.2014.01.007

Zhen, F., Y. Lan, B. Yan, W. Zhang, and Z. Wen. 2013. Hemogenic endothelium specification and hematopoietic stem cell maintenance employ distinct Scl isoforms. *Development.* 140:3977–3985. http://dx.doi.org/10.1242/dev.097071

Zhu, J., R. Garrett, Y. Jung, Y. Zhang, N. Kim, J. Wang, G.J. Joe, E. Hexner, Y. Choi, R.S. Taichman, and S.G. Emerson. 2007. Osteoblasts support B-lymphocyte commitment and differentiation from hematopoietic stem cells. *Blood.* 109:3706–3712. http://dx.doi.org/10.1182/blood-2006-08-041384